Department of Forest Products Technology

Supported ultrathin films and non-woven fibre mats from polysaccharide containing bicomponent polymer blends

Laura Taajamaa

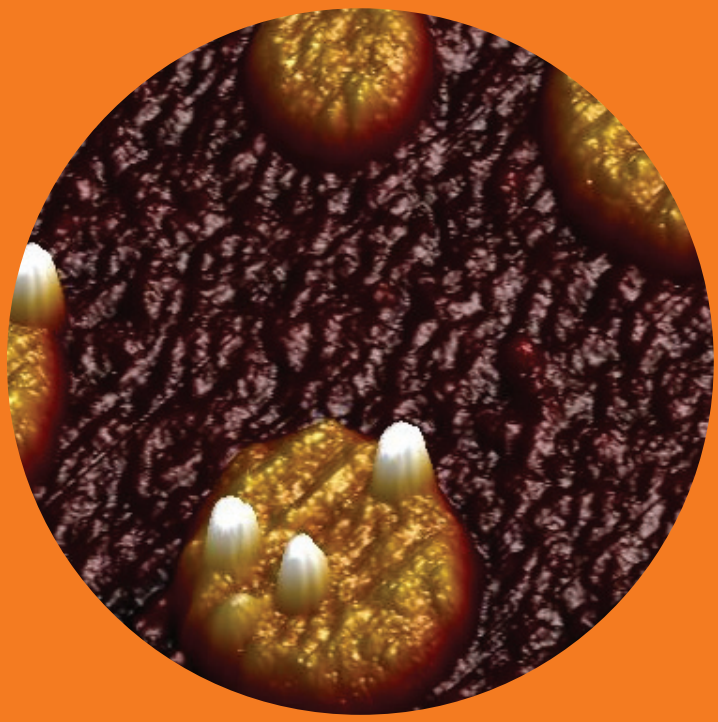

A!

DOCTORAL DISSERTATIONS

Aalto University publication series
DOCTORAL DISSERTATIONS 87/2014

Supported ultrathin films and non-woven fibre mats from polysaccharide containing bicomponent polymer blends

Laura Taajamaa

A doctoral dissertation completed for the degree of Doctor of Science (Technology) to be defended, with the permission of the School of Chemical Technology, at a public examination held at the Auditorium Puu2 of the Aalto University School of Chemical Technology (Espoo, Finland) on the 16th of July 2014 at 12 noon.

Aalto University
School of Chemical Technology
Department of Forest Products Technology
Forest Products Surface Chemistry

Supervising professor
Professor Janne Laine

Thesis advisors
Dr Eero Kontturi
Professor Orlando Rojas, Aalto University and North Carolina State University, United States of America

Preliminary examiners
Professor Takuya Kitaoka, Kyushu University, Japan
Professor Denise F. S. Petri, University of São Paulo, Brazil

Opponent
Professor Stephen Eichhorn, University of Exeter, United Kingdom

Aalto University publication series
DOCTORAL DISSERTATIONS 87/2014

ISBN 978-952-60-5730-9
ISBN 978-952-60-5731-6 (pdf)
ISSN-L 1799-4934
ISSN 1799-4934 (printed)
ISSN 1799-4942 (pdf)
http://urn.fi/URN:ISBN:978-952-60-5731-6

Unigrafia Oy
Helsinki 2014

Finland

441 697
Printed matter

Author
Laura Taajamaa

Name of the doctoral dissertation
Supported ultrathin films and non-woven fibre mats from polysaccharide containing bicomponent polymer blends

Publisher School of Chemical Technology

Unit Department of Forest Products Technology

Series Aalto University publication series DOCTORAL DISSERTATIONS 87/2014

Field of research Forest Products Chemistry

Manuscript submitted 27 March 2014 **Date of the defence** 16 July 2014

Permission to publish granted (date) 13 May 2014 **Language** English

☐ **Monograph** ☒ **Article dissertation (summary + original articles)**

Abstract

Compared to petroleum based chemicals, polysaccharides enable sustainable approaches and environmentally friendly products. Cellulose is the most abundant polymer in the biosphere and it has recently gained wide interest as a source for nanomaterials with remarkable strength and liquid crystalline properties. This work is aimed at gaining knowledge on ultrathin cellulose films on solid supports. The morphology, formation and modification of ultrathin cellulose films were investigated from the fundamental point of view. In addition to novel non-covalent surface modification methods in ultrathin cellulose films, the resulting films were converted from 2D structures into 3D fibre systems.

Forming functional systems with high surface-to-volume and aspect ratios is an important driver in nanoscience. One challenge is creating nano- and micronscale structures on ultrathin polymer films. A straightforward bottom-up approach to pattern polymeric films is using the spin coating technique for binary polymer blend solutions. Phase separation in the ultrathin films formed results from thermodynamic instabilities generated during the rapid spin coating process and surface patterns emerge from the interactions between the polymer blend components, the solvent and the substrate. The polymer blend films can be used in fundamental studies as well as in applications spanning from controlled drug release to organic light emitting diodes.

Ultrathin blend films consisting of cellulose and a hydrophobic polymer were introduced, followed by a method to quantitatively modify the surface chemistry and morphology of the ultrathin cellulose films. A cellulosic template for nanoparticle immobilisation was created. The tailored properties were achieved by the choice of the solution blend ratio used in spin coating. The second part of the thesis focused on the blends of two polysaccharide derivatives. The construction of bicomponent cellulose films with phase-specific pore formation was discussed, along with reasons explaining the genesis and evolution of the given morphologies. Finally, a method to prepare cellulose derivative blend fibre mats by electrospinning that could be selectively modified after fibre formation was unveiled.

This thesis represents a fundamental endeavour to deepen our understanding of various polymer blend architectures. It encompassed a set of investigations related to the construction and modification of supported ultrathin films and non-woven fibre mats from blends containing cellulose derivatives. It is expected that results presented in this interdisciplinary area of science can pave the way for the increasing cooperation, enabling future discoveries.

Keywords polysaccharide, cellulose, cellulose derivative, polymer blend, spin coating, electrospinning, ultrathin film, fibre mat, modification

ISBN (printed) 978-952-60-5730-9 **ISBN (pdf)** 978-952-60-5731-6

ISSN-L 1799-4934 **ISSN (printed)** 1799-4934 **ISSN (pdf)** 1799-4942

Location of publisher Helsinki **Location of printing** Helsinki **Year** 2014

Pages 145 **urn** http://urn.fi/URN:ISBN:978-952-60-5731-6

Tekijä
Laura Taajamaa

Väitöskirjan nimi
Polysakkaridipohjaisten polymeeriseosten ohutkalvoista ja kuitumatoista

Julkaisija Kemian tekniikan korkeakoulu

Yksikkö Puunjalostustekniikan laitos

Sarja Aalto University publication series DOCTORAL DISSERTATIONS 87/2014

Tutkimusala Puunjalostuksen kemia

Käsikirjoituksen pvm 27.03.2014 **Väitöspäivä** 16.07.2014

Julkaisuluvan myöntämispäivä 13.05.2014 **Kieli** Englanti

☐ **Monografia** ☒ **Yhdistelmäväitöskirja (yhteenveto-osa + erillisartikkelit)**

Tiivistelmä

Verrattaessa öljypohjaisiin kemikaaleihin, polysakkaridit ovat askel kohti ympäristöystävällisempiä ja kestävän kehityksen mukaisia tuotteita. Selluloosa on yleisin biopolymeeri ja viime aikoina se on herättänyt kasvavaa kiinnostusta nanomateriaalien raaka-aineena muun muassa erinomaisten mekaanisten ja optisten ominaisuuksiensa ansiosta. Tämän työn tarkoituksena oli tuottaa perustietoa selluloosan ohutkalvoista, tarkemmin niiden pinnan morfologiasta, sen kehittymisestä sekä kalvojen ominaisuuksien muokkaamisesta. Kehitettyjen pinnanmuokkausmenetelmien lisäksi väitöskirjassa siirrettiin kaksiulotteisten ohutkalvojen pinnanmuodot kolmiulotteisiin kuitumattoihin.

Nanotieteen yhtenä tavoitteena on muodostaa hierarkkisia rakenteita, joilla on suuri pinta-ala niiden tilavuuteen nähden. Haasteena on esimerkiksi nano- ja mikroskaalan kuvioiden rakentaminen ohuisiin polymeerikalvoihin. Eräs yksinkertainen lähestymistapa on käyttää spin coating –tekniikkaa polymeerien seoksille. Kuviot muodostuvat ohutkalvon pinnalle substraatin, liuottimen sekä polymeeriseoksen komponenttien vuorovaikutuksesta, kun liuottimen haihtuminen sysää kalvon pois termodynaamisesta tasapainosta. Polymeerien seoskalvojen sovelluskohteet vaihtelevat perustutkimuksesta hohtodiodeihin ja lääkeaineiden annosteluun.

Väitöskirjan alussa paneuduttiin selluloosan ja vettä hylkivän polymeerin seoskalvoihin. Työssä kehitettiin menetelmä kyseisten seosohutkalvojen pinnan kemian ja morfologian muokkaamiseen. Ominaisuuksien muokkausta hallitaan ja säädellään alkuperäisen polymeeriliuoksen komponenttien seossuhdetta säätämällä. Lisäksi tutkittiin nanopartikkeleiden kiinnittämistä määrättyihin osiin selluloosakalvoa. Työn jälkimmäisessä osassa keskityttiin kahden selluloosajohdannaisen seoskalvoihin, joissa havaittiin toisen seoskomponentin alueelle keskittyneitä huokosia. Lisäksi syvennyttiin ilmankosteuden vaikutukseen morfologian muodostumisessa ja sen kehittymisessä. Lopuksi työssä valmistettiin selluloosajohdannaisten seoskuitumattoja sähkökehruulla. Työssä tutkittiin myös kuitumaton ominaisuuksien muokkaamista yksittäistä selluloosajohdannaista muokkaamalla.

Väitöskirjassa syvennettiin ymmärtämystä erilaisista polymeeriseosten muodostamista rakenteista. Työ koostui neljästä osasta, joissa paneuduttiin selluloosan johdannaisia sisältävien polymeeriseosten ohutkalvojen ja kuitumattojen rakenteen muodostumiseen sekä muokkaukseen. Tämän tutkimuksen tarkoituksena oli myös helpottaa selluloosatutkimuksen poikkitieteellistä yhteistyötä.

Avainsanat polysakkaridi, selluloosa, selluloosan johdannainen, polymeeriseos, spin coating –tekniikka, sähkökehruu, ohutkalvo, kuitumatto, muokkaus

ISBN (painettu) 978-952-60-5730-9 **ISBN (pdf)** 978-952-60-5731-6

ISSN-L 1799-4934 **ISSN (painettu)** 1799-4934 **ISSN (pdf)** 1799-4942

Julkaisupaikka Helsinki **Painopaikka** Helsinki **Vuosi** 2014

Sivumäärä 145 **urn** http://urn.fi/URN:ISBN:978-952-60-5731-6

PREFACE

This study was carried out between 2008 and 2012 at the Department of Forest Products Technology at Aalto University (formerly Helsinki University of Technology). Funding from the Doctoral Programme for Biomass Refining (BIOREGS), Lignocell and Tailorpap projects, the Finnish Funding Agency for Innovation (TEKES), Academy of Finland and industrial partners is gratefully acknowledged. Personal travel grants and support for international exchange from Emil Aaltonen Foundation, TES – Tekniikan edistämissäätiö and Magnus Ehrnrooth foundation are also highly appreciated.

My supervisor Janne is thanked for his support, convincing me to continue my studies and providing a comfortable situation to do research, i.e., for not to have to worry about funding unlike many of my peers. I am privileged to have had Eero as my instructor. Not only because he is passionate about his work and cellulose and taught me a lot about science, but because the great and easy-going person he is. "Let's take it easy, things will work out!" And indeed, they eventually always did. Furthermore, I wish to express my sincere thanks to my second instructor Orlando for his wholehearted support, never-ending optimism and confident attitude. I could always rely on his help even though most of the time we were separated by an ocean. I also want to thank him and Janne for the wonderful opportunity and experience to visit his group. Additionally, my co-author Kirsi Yliniemi is thanked for her crucial input in my last paper.

Professors Takuya Kitaoka and Denise Petri are thanked for the thesis pre-examination, positive attitude, valuable comments and insightful suggestions that helped in refining the thesis! Joe Campbell is thanked not only for the linguistic revision of the thesis but also for providing additional comments that improved the quality of this thesis.

All past and present colleagues are thanked for creating a wonderful working atmosphere! Special thanks to the research groups of Janne, Tapani, Eero, Monika and Adrian. Aila, Anu, Marja, Risu and Rita are thanked for running the labs and lending a helping hand in many occasions. Pena is thanked for his help in IT matters and Ari&Timo are kindly thanked for the numerous times you opened office door to the forgetful me. Tuomas and Katri – the original summer 2005 Puljake gang, without you I probably would not have returned. Thank you for all the happy moments spent together. Tiina and Elli, my deepest thanks for accepting me as I am and still calling me your friend! Miroslaav Sushi; you are one of those persons who make the world a better place just by your presence and smile! I would like to express my sincere thanks for our friendship and great times, but also apologies for the occasional grumpy moments. Mikko Nieminen Georgiasta - thank you for the laughs, stupid jokes and your friendship. Hannes and Niko are thanked for their special sense of humour. Hannes is additionally thanked for trusting me his car&infant

carrier, for his phenomenal prediction skills and helping out in the lab. Tiina, Elli, Karo, Paula, Raili, Katri, Minna and Anna; huge thanks for sharing the ups and downs on the path to the doctoral degree! Tero is acknowledged for the Ruuhkabussi and happy smiles! Katri, Karo, Elina, Raili, Anni, Hannes, Emmi, Jonna, Reeta, Maija, Elli, Minna, Kati, Anu and Juuso – thanks for the happy lunch&coffee breaks either at the PuuII cafeteria and/or at the coffee room. Naveen is recognised for courageously inviting a bunch of Finns into his home for dinner. I have enjoyed these evenings a lot! Special thanks to Ola, Elli and Arcot for sharing an office with possibly one of the messiest persons in the world. For Elli, who always has her paper in neat piles, this must have been a torment beyond belief… my apologies also on the "mummified apple" found under my cupboard some months after I had started my maternity leave..

Part of this thesis work was performed at the Departments of Forest Biomaterials at North Carolina State University. Past and present members of the colloids and interfaces group, CIG, are thanked for the welcoming atmosphere, lending a helping hand and friendship. Special thanks go to Ingrid for hosting me, Barbara, Sole, Carlos I, Kelley, Justin and Xiaomeng.

All my friends are acknowledged for providing numerous fun occasions during the years! My chemists a.k.a. "Firma" are thanked for their continuous support and friendship throughout the years at the university and various stages of life. Special thanks to Outi, Annukka, Taru and Ansu for inspiration and support in matters related to finishing a doctoral degree.

My extended family and relatives are thanked for the support and many memorable moments throughout the years. I want to thank Hanna and Harri for your unconditional support during my life and studies. You have offered both material and immaterial resources without saving your troubles. My gratitude goes to Hanna for providing me a great environment to grow up and to study.

Last but not least I want to express my heartfelt thanks to Mauno and Ella for bringing occasional chaos, but mostly happiness and smile in my life. It is an enormous privilege that I may share my life with you! Mauno: your flexibility and support especially during the last months of the thesis writing have been outstanding. M, E & E: you are my everything - thank you for every day!

Otaniemi, June 3rd 2014

Laura

LIST OF PUBLICATIONS

This thesis is mainly based on the results presented in four publications which are referred with Roman numerals in the text.

Paper I Nyfors, L., Suchy, M., Laine, J., Kontturi, E. (**2009**) Ultrathin Cellulose Films of Tunable Nanostructured Morphology with a Hydrophobic Component. *Biomacromolecules* 10 (5), 1276-1281.

Paper II Taajamaa, L., Rojas, O. J., Laine, J., Yliniemi, K., Kontturi, E. (**2013**) Protein-assisted 2D assembly of gold nanoparticles on a polysaccharide surface, *Chem. Commun.*, 49 (13), 1318-1320.

Paper III Taajamaa, L., Rojas, O. J., Laine, J., Kontturi, E. (**2011**) Phase-specific pore growth in ultrathin bicomponent films from cellulose-based polysaccharides. *Soft Matter*, 7 (21), 10386-10394.

Paper IV Taajamaa, L., Kontturi, E., Laine, J., Rojas, O. J. (**2012**) Bicomponent fibre mats with adhesive ultra-hydrophobicity tailored with cellulose derivatives. *J. Mater. Chem.* 22 (24), 12072-12082.

Author's contribution to the appended joint publications:

I-IV Laura Taajamaa (née Nyfors) was responsible for the experimental design, performed the main part of the experimental work, analysed the corresponding results, and wrote the manuscripts.

LIST OF KEY ABBREVIATIONS

AFM	atomic force microscopy
AGU	anhydroglucose unit
ATR	attenuated total reflection (detection)
AuNP	gold nanoparticle
CA	contact angle
CAM	contact angle measurement
CellA	cellulose acetate
CTA	cellulose triacetate
EIP	effective interface potential
FEM	free energy of mixing
T_g	glass transition temperature
DS	degree of substitution
DP	degree of polymerization
M_w	molecular weight
NP	nanoparticle
PS	polystyrene
QCM-D	quartz crystal microbalance with dissipation monitoring
RH	relative humidity
SEM	scanning electron microscopy
TMSC	trimethylsilyl cellulose
WCA	water contact angle
XPS	x-ray photoelectron spectroscopy

TABLE OF CONTENTS

"*Nainen tarvitsee elämässään kahta asiaa: huumoria ja punaiset korkokengät. -- Tohtorintutkinto on hyväksi muttei välttämätön.*"

"*A woman needs two things in her life: a sense of humour and red high heels: -- a doctoral degree is an asset, but not a necessity.*"

Riikka Pulkkinen, in her novel "True"

1. INTRODUCTION AND OUTLINE OF THE STUDY

Nanoscience is a discipline that studies the phenomena and manipulation of materials at atomic, molecular and macromolecular scales, *i.e.*, with the smallest dimensions in the range from one to one hundred nanometres. The term is a fusion of the words "nano" (originating from Greek *nanos* or Latin *nanus* – dwarf), often used as a prefix denoting a billionth (1×10^{-9}) and "science" (originating from Latin *scientia* – knowledge). Nanotechnology, on the other hand, is an engineering field that applies nanoscience to fabricate products or processes based on nanoscale components. Nanoscience and nanotechnology operate at the fascinating interface between physics, chemistry and biology. Commonly, they are attributed with great potential, and subsequently are attracting increasing interest. The advent of the nano boom occurred in the latter half of the 20th century;[1,2] however, many nanosized materials have been utilised for centuries.[3,4]

Creating functional systems with high surface-to-volume and aspect ratios is an important driver in nanoscience. One of the endeavours is implanting diverse nano- and microscale architectures on ultrathin polymer films. One way to categorise the methods to achieve this task is to divide them into top-down and bottom-up techniques. The former methods begin with a block of material which is then deconstructed to a small scale structure while the latter techniques utilise inherently small building blocks assembled to construct a desired material.[5]

An effortless bottom-up way to pattern polymeric films utilised in this work involves the spin coating process for binary polymer blend solutions. This patterning technique is based on the thermodynamic instability generated during the rapid spin coating process and surface patterns emerge from the interactions between the polymer blend components, the solvent and the substrate. Besides their fundamental interest, polymeric bicomponent films can be utilised in a range of applications from organic light emitting diodes and photovoltaics to templates for controlled drug release. The properties of polymer blends in bulk are rather well established, but the presence of the interface causes constraints.[6,7] For instance, the phase separation behaviour during the quench of solvent evaporation in spin coating polymer blends is still not fully understood.

As we strive towards more sustainable and environmentally friendly processes and products, polysaccharides have the potential to play a key role. Cellulose is the most abundant polymer in the biosphere. Approximately 10^{15} kg of cellulose is produced annually in nature[8]. Throughout history, cellulose has played an important part in our lives whether as an energy source, facilitating communication or providing shelter. Recently, cellulose has drawn wider interest as a native source for nanomaterials with unusual characteristics, such as remarkable strength properties and liquid crystalline properties.[9] The utilization of cellulose in ultrathin films is interesting, but not yet a widely explored field. Typically, nanocellulosic objects are formed top-down processes that break the native structures. In contrast, the presented spin coating process uses blends of solutions containing hydrophobic cellulose derivatives. It offers a straightforward way to prepare micro- and nanoscopic cellulose architectures. Expanding the scope of 2D films into 3D fibre networks widens the field of conceivable applications.

The overarching goal of this thesis is to gain knowledge of the development of ultrathin cellulose films supported on solid substrates. The morphology, formation and modification of ultrathin cellulose films are investigated from a fundamental point of view. Surface functionalization of cellulose films is demanding due to the often counterintuitive response of cellulose to covalent modifications. In addition to novel non-covalent surface modification methods for cellulose ultrathin films, emphasis in this thesis is also placed to translate the 2D film architectures formed into 3D fibre mats. The use of renewable and widely available polysaccharides endorses the sustainable aspect of such nanotechnology efforts.

The first part of the thesis focuses on bicomponent ultrathin films of cellulose and a hydrophobic polymer. **Paper I** presents a method to quantitatively modify the surface chemistry of ultrathin cellulose films during film preparation. Tailorable hydrophobic functionalization of hydrophilic polysaccharide films was achieved with an effortless “bottom-up” approach, without covalent modification nor the complexity of lithographic techniques. **Paper II** showcases a facile method to immobilize nanoparticles (NPs) on the polysaccharide surfaces (from **Paper I**) with micro- and nanoscale lateral precision. The surface morphology of the films and the amounts of assembled NPs were easily tunable. Morphologically, the structures decorated with NPs

ranged from cellular network structures to discrete circular patches on the polysaccharide surface.

The latter part of the thesis concentrates on blends of two cellulose derivatives. The construction of bicomponent polysaccharide films with phase-specific pore formation was introduced in **Paper III**. Furthermore, the reasons behind the genesis and the morphological evolution of the films were scrutinized. An attempt to transfer the interesting 2D morphologies of films into 3D fibre mats is reported in **Paper IV**. This effort presents a method to fabricate bicomponent cellulose derivative non-woven fibre mats that can be modified after fibre formation through the conversion of the respective components to cellulose. Scheme 1 represents an overview of the main themes of this work and summarises the relations of the papers.

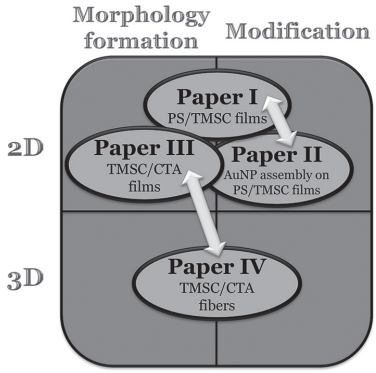

Scheme 1. Summary of this compilation dissertation and the papers included.

Nanoscience is genuinely a cross-disciplinary area; the physics and chemistry of matter at the nanoscale are pertinent to scientific disciplines from chemistry and physics to biology, engineering and medicine. Generally, the present work aims at making a contribution in paving the way for the cross-disciplinary cooperation, which is bound to increase in the future, as more scientists enter the fascinating world of polysaccharides and cellulose.

2. BACKGROUND

2.1 Polysaccharides

Carbohydrates are biomolecules that constitute most of the organic matter in the biosphere. They have a variety of functions, from acting as energy storage, fuels, metabolism intermediates, building blocks for RNA and DNA, to meditating cell interactions and as structural components in plants. Monosaccharides are molecules composed of carbon, hydrogen and oxygen and they usually contain from three to nine carbon atoms and two or more hydroxyl groups. Monosaccharides vary not only in size but also in stereochemical configuration. Monosaccharides assemble into oligo- and polysaccharides through glycosidic bonds: *i)* di- and trisaccharides comprise of two and three monosaccharides, respectively; *ii)* oligosaccharide is an umbrella term for carbohydrates in between simple monosaccharides and large polysaccharides and they usually contain from two to ten monosaccharides; and finally *iii)* polysaccharides contain numerous monosaccharides.[10]

Polysaccharides serve as a nutritional reserve and as structural elements in the plant and in bacterial cell walls. Nature has fine-tuned the structure (*e.g.* linear *vs*. branched) and composition depending on its use. Polysaccharides which include only one type of monosaccharide are known as homopolysaccharides and those with different repeating units are called heteropolysaccharides. Examples of common polysaccharides are glycogen and starch, the storage forms of glucose in animal and plant cells, respectively.[10] The polysaccharide essential for this work, cellulose, is presented in the following paragraphs.

2.2 Cellulose

Cellulose, the main component in woody plants, is almost an inexhaustible polymeric material with a unique structure and properties. During the last few decades there has been an increased interest towards cellulose, cellulose derivates and other polysaccharides. This is partly due to a growing need for biodegradable, renewable and non-petroleum based materials, in addition to sustainable and environmentally friendly processes. Furthermore, the general

increased interest in nanotechnogy has had an effect given the inherent nanosize of cellulose fibrils. The peculiar properties, *e.g.*, large surface-to-volume ratio and high aspect ratio, of these fibrils have secured wider interest in the scientific community.

2.2.1 The molecular and supramolecular structure

Cellulose is linear syndiotactic homopolysaccharide comprising of D-anhydrogluco-pyranose units (AGUs) linked together *via* β-(1→4)-glycosidic bonds (Figure 1). The amount of chair-conformed AGUs determines the degree of polymerization (DP), however, the dimer cellobiose is the repeating unit. Although hydrophilic through hydroxyl groups, cellulose is insoluble in water unlike the monosaccharide glucose. Conventionally, this has been ascribed to extensive hydrogen bonding; however, an alternative view that is gaining support is based on hydrophobic interactions due to the amphiphilic nature of cellulose, which contribute significantly to water insolubility.[11] Cellohexaose (DP of 6) is the longest water-soluble oligosaccharide. Already a molecule with thirty AGUs can represent polymeric cellulose both in structure and in other characteristics.[12] The DP of cellulose is highly dependent on the origin and pre-treatment. Native cellulose has DP *circa* 6000-9500.[8]

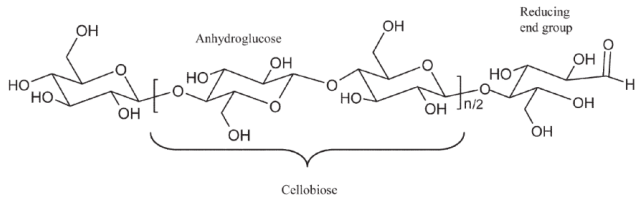

Figure 1. The molecular structure of cellulose. AGU is the monomer and cellobiose is the dimer and repeating unit of cellulose. Cellulose chains have direction due to the different end-groups. Reproduced from Ref. 15 with permission of The Royal Society of Chemistry.

The molecular structure of cellulose is simple but the most exceptional properties are due to its supramolecular structure. Cellulose chains have an intense tendency to aggregate, and cellulose biosynthesis begins with the assembly of the chains into bundles, or elementary fibrils (Figure 2). The cellulose molecules in the elementary microfibrils are arranged in parallel with a double twist symmetry along their length. Elementary fibrils aggregate further into microfibril bundles which in turn assemble into lattices within the fibre cell wall. The high degree of order results in a crystalline and stable

structure. Cellulose has various polymorphs and the most significant forms, cellulose I (parallel) and II (anti-parallel stacking of the molecules) represent native and regenerated cellulose, respectively. The microfibrils lattices also contain disordered regions arising from imperfect packing and interactions with other non-cellulosic polysaccharides[13]. These disordered regions are often described as amorphous cellulose.[14]

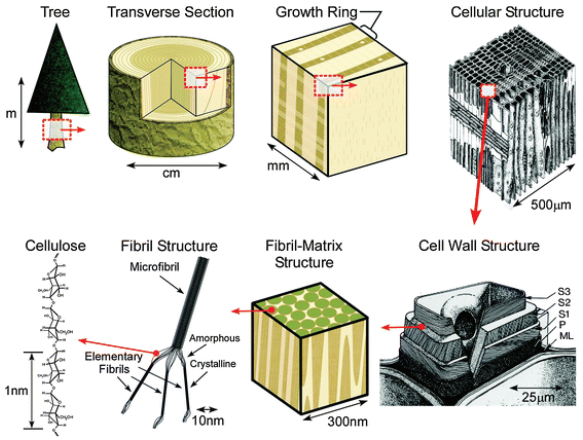

Figure 2. The hierarchical structure and dimensions of the various parts of a tree.[16]

2.2.2 Cellulose derivatives

Cellulose cannot be melted for processing in a fashion similar to many synthetic polymers by virtue of its degradation temperature and even glass transition temperature (T_g) being so close to its melting temperature (T_m). This has steered researchers to study a fairly challenging topic, the chemical modification of cellulose. Strong stability in nature, highly ordered supramolecular structures and the resulting insolubility in common solvents are the reasons why chemical reactions do not often proceed in an intuitive fashion with respect to familiar pathways in organic chemistry. Thousands of publications have been written exclusively about the chemical modification of cellulose (for review see, *e.g.*, Refs. 17-19 and the references therein). Different forms of cellulose – native fibres, regenerated films or bacterial cellulose fibrils, for example – require different means of modification, or at least their extent of reactivity differs.

The three hydroxyl groups in each AGU are the main reactive sites in the cellulose molecule. The hydroxyl groups can be partially or fully reacted with various reagents to provide derivatives with useful properties. Conventional

chemical methods to modify cellulose include esterification (R-CO-OR'),[20,21] etherification (-OR)[21] and oxidation of the hydroxyl groups.[19] Esterification of cellulose is the main route of conventional modification. Cellulose xanthate represents a majority of the cellulose derivatives produced and it has been produced industrially along with cellulose nitrate and cellulose acetate (CellA) from the late 19th century. These derivatives are utilised in, *e.g.*, cellulose processing, explosives and cigarette filters, respectively. From the scientific point of view there are a variety of compounds and material properties to be achieved and it forms a bridge between the general and a special branch of organic chemistry. Cellulose etherification dates back to the beginning of the 20th century, and today carboxymethyl cellulose is commercially the most significant product. The oxidation of hydroxyl groups in cellulose introduces carboxy, aldehyde and keto groups; however, controlled modification is not usually achieved with this route. Mastering oxidation reagents and reaction conditions is problematic and depolymerisation almost inevitably occurs. With the conventional methods of organic chemistry, cellulose modification may either take place in a homogeneous or heterogeneous medium. The polymer blend precursor trimethylsilyl cellulose (TMSC) in this thesis was prepared with homogenous modification. In the case of nanocellulosic materials, heterogeneous methods are the only applicable ones since the dissolution of cellulose, required for homogeneous conditions, destroys the morphology of nanocellulosics. The means to modify cellulosic material include, for instance, polysaccharide adsorption,[22] click chemistry,[23] enzymatic treatment[24] and polyelectrolyte multilayers and complexes[25]. Also, thin film specific modification paths exist.[19] Cellulose derivatives most relevantly linked to this thesis are TMSC and CellA and they are concisely discussed below.

Trimethylsilyl cellulose and cellulose acetate

Preparing soluble derivatives by silylation can provide a route which can significantly broaden the scope of applications. Cellulose silyl ethers with varying degree of substitution (DS) and regioselectivity can be generated.[17] They are thermally stable and are usually characterised by increased lipophility and hydrophobicity.[19] As TMSC (DS<2.5) dissolves in common non-polar organic solvents, *e.g.*, chloroform and toluene, it can be blended, with, for instance synthetic hydrophobic polymers.[26,27] The organosolubility of TMSC decreases with increasing DS. Mormann and Demeter have reported that the molar mass and not the DS defines the solubility when DS>2.5. [28]

Thermal properties are also altered when DS approaches 3.[28] The crystallinity index of TMSC has been described to increase with decreasing DS.[29] Pawlowski *et al.* reported the lyotropic and thermotropic behaviour of TMSC.[30] Decomposition was observed to begin at 323°C. Cooper *et al.* stated that while TMSC can be melted without significant decomposition in oxygen-free conditions, already 2% of oxygen triggered decomposition below 320°C.[31]

CellA has been used in films, fibres, lacquers, moulding and extrusion compounds.[32] CellA is typically produced from cotton linters or wood pulp with a catalyst in acidic, water-free conditions. This leads to a decrease in the DP, down to approximately 300. The reaction first proceeds to full substitution (DS 3 or cellulose triacetate (CTA)), and the CTA is then deacetylated in homogeneous conditions to obtain polymers with various DS and uniform distributions of acetate groups. Commercial CellA is always heterogeneous, *i.e.*, the position of the acetate groups cannot be selected or tailored and it could be regarded as a co-polymer of DS 1, 2 and 3. The melting point of CellA is *circa* 227°C (at DS = 2.45)[33] and the solubility of CellA varies according to the DS (Table 1).[19,32] Since the 1990s, an increased interest in CellA and other biodegradable plastics, designed to be degraded by microorganisms in waste landfills, has arisen as an alternative to petroleum-based polymers. The rate of CellA biodegradation depend on the DS,[34] the degradability by cellulase improves with decreasing DS.[35]

Table 1. The solubility of CellA according to the DS and substitution pattern. Adapted from Refs. 19 and 32.

Liquid	**DS solubility range for CellA**	
	in C-2/-3/-6 position	in C-2/-3 position
Water	0.8-1.0	Insoluble
Dimethylformamide	1.8-2.7	1.3-2.8
Acetone (1 % water)	2.3-2.6	2.5-2.6
Pyridine	0.8-2.7	1.2-2.8
Pyridine/Water (1:1 v/v)	0.6-2.0	1.2-1.6
Ethyl lactate	1.6-2.7	2.6-2.8
Chloroform	2.8-3.0	

2.3 Supported ultrathin films

The motivation for ultrathin film research is two-fold: they are utilised in fundamental research as model surfaces with controlled chemical and morphological features, as well as in the search for novel materials. In addition

to the fact that modern analytical tools often require smooth samples, model surfaces offer a way to study complex phenomena, *e.g.*, fibre interactions during papermaking, in a simplified manner. The definition of an ultrathin film has varied in the course of time and in between disciplines. In this work, an ultrathin film is specified as film with a thickness less than one hundred nanometres.

Ultrathin film modification is a widely studied topic in nanoscience. The modification paths are divided into top-down methods, *e.g.*, various lithographic techniques, nanocontact printing and writing and molding, and bottom-up techniques, *e.g.*, layer-by-layer deposition, surface instabilities, patterns with block-copolymers and DNA self-assembly, to name only a few. The straightforward bottom-up modification route applied in this thesis is spin coating binary polymer blend solutions. Similar films have been used in, for instance, antireflective coatings[36] and conductive polymer films[37].

2.3.1 Preparation

Several methods have been applied to prepare ultrathin supported films. They range from layer-by-layer[38] and spin coating[39] to chemical vapour deposition[40] and Langmuir-Blodgett[41] (LB) or horizontal LB also known as Langmuir-Shaeffer (LS) deposition and further to dip coating[42] and solvent casting[42]. The technique most relevantly linked to this thesis, spin coating, is presented in detail.

Spin coating

The spin coating technique has established widespread use in academia and industry (for review, see *e.g.* Ref. 43 and references therein). Spin coating is a straightforward and fast technique to prepare supported ultrathin films from dispersed or dissolved materials. The only prerequisite is that the coating solution has to wet the substrate. The films acquired are not in equilibrium; they adopt a metastable morphology after solidification due to rapid solvent evaporation.[44] A typical spin coating setup is shown in Figure 3: the solid support is fixed to a chuck which is spun at a chosen rate, usually between 1000 to 6000 rpm.

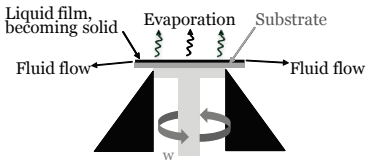

Figure 3. Spin coating setup.

Emslie and co-workers were the first to formulate a spin coating theory in 1958.[45] The theory was later improved by Acrivos *et al.*[46] and Meyerhofer[47]. Bornside *et al.* divided spin coating into four stages: deposition, spin-up, spin-off and evaporation.[48] Deposition takes usually place on a static substrate and in the spin-up, the substrate is accelerated to the spinning speed leading to the ejection of a majority of the solution. In the spin-off, the fluid flow continues until the viscosity of the solution increases rapidly and the evaporation stage begins. From that time forward, film thinning occurs *via* evaporation. The spin-off and evaporation stages determine the film thickness and roughness, respectively.

Several parameters related to the solution and the substrate play a role in film formation during spin coating. The concentration of the original polymer solution and thus its viscosity are key factors in determining the film thickness. Typically the higher the concentration, the thicker and rougher the film.[49] Even though precise knowledge is seldom needed in advance, the film thickness (h) can be estimated by,[47]

$$h_\infty \propto \omega^{-\frac{1}{2}} \eta^{\frac{1}{3}} c_0, \qquad (1)$$

where ω denotes spinning speed and η and c_o, the viscosity and the concentration of the initial spinning solution, respectively. Along with the aforementioned parameters, the choice of solvent effects film roughness: a solvent with low vapour pressure produces smoother films[50].

2.3.2 Ultrathin polysaccharide films

Biodegradable polymers not only play a role in solving the problems related to landfills and petroleum reserves, they are also potential candidates for, *e.g.*, medical applications[51-53]. Ultrathin chitosan films have beem suggested to have prospects in sensor and coating applications.[54] Anti-adhesive heparin films have been prepared, for example, with the LbL technique.[55,56] Lately, also

various oligo- and polysaccharide architectures[57,58] have gained increased interest in, *e.g.*, analytics,[57-59] drug release[60] and cell encapsulation[61].

As mentioned above, cellulose is an important polysaccharide; however, ultrathin films prepared from cellulose are rather an underexplored field. Ultrathin cellulose films can be divided into native and regenerated cellulose films.[42] Native films are made from colloidal suspensions of cellulose micro or nanofibres (for example, nanofibrils[62]) or their fragments (*e.g.*, cellulose nanocrystals[63]). Regenerated ultrathin films can be prepared either directly from dissolved cellulose[64,65] or *via* unstable derivatives. Direct dissolution of cellulose is rather laborious and the solvents utilised are complex systems, *e.g.* dimethyl acetamide/lithiumchloride (DMAc/LiCl)[66] and N-methylmorpholine N-oxide/water[67]. Moreover, the utilisation of the DMAc/LiCl solvent requires additional treatment after film preparation to remove salt and excess DMAc (traces are left due to its low vapour pressure).[49]

Cellulose derivatives, when soluble, in, for example, toluene and chloroform, enable easy ultrathin film preparation. Studies of ultrathin cellulose derivative films prepared from derivatives other than TMSC are scarce. Lua *et al.* reported films from ethylcellulose (EC), hydroxypropyl methylcellulose (HPMC) and their blends; however, film thickness varied from ~120 nm to ~1000 nm.[68] Also, the reported CellA,[69,70] cellulose acetate propionate, cellulose acetate butyrate and carboxymethylcellulose acetate butyrate films are rather thick.[71] Recently, Palla-Papavlu *et al.* utilised matrix-assisted pulsed laser evaporation to create ultrathin EC and HPMC films.[72]

When utilising derivatives for the dissolution of cellulose it is imperative that the regeneration to cellulose is straightforward and reproducible. Both hydrophobised cellulose derivatives used in this work, TMSC and CTA, can easily be regenerated to cellulose with an aqueous gas phase treatment (Section 3.2.1.). Ultrathin films used in this work were regenerated derivative films, so a brief introduction on previous efforts is presented below.

The pioneering work by Schaub *et al.* in 1993[26] presented the preparation of homogenous and smooth ultrathin LB TMSC films as well as the *in-situ* gas phase regeneration to cellulose.[73] Next, film characterisation was extended; the effect of the LB process parameters was studied in addition to film modification, and its application as a model system for adsorption studies.[73] Holmberg *et al.*[74] refined the method even further and employed the films for

surface force measurements. Spin coated regenerated films were first introduced already in 2000 by Geffroy and co-workers;[75] however, they did not gain wider attention until Kontturi *et al.* scrutinised the films and fine-tuned the method.[50,76] There, the films were characterised *via* atomic force microscopy (AFM), x-ray photoelectron spectroscopy (XPS), infrared spectroscopy (IR) and ellipsometry. A comparative study by Rossetti *et al.* stated that films prepared with either LB and spin coating are equally smooth and reproducible, although LB films exhibited denser structure and, moreover, controlling the LB process was more straightforward.[77] Recently also, Mohan *et al.* studied the partial and full regeneration of spin coated TMSC films.[78]

The novel advances in cellulose films are related to analytical tools, novel preparation methods (namely new solvents) and the creation of multifaceted films with controlled morphologies.[15,42] Preparing cellulosic films with various patterns can be achieved *via* microspotting,[79] open films,[70,80-82] breath figures,[83] photolithography,[81] soft lithography,[84] enzymes[84] and polymer blends[27] among others. Creating patterned films forms a basis for this work.

2.4 Polymer blends and phase separation

A polymer blend is a mixture of at least two macromolecular substances,[85] and the purpose of a polymer blend is to achieve characteristics not available from the individual constituents or from other materials. Since the synthesis of novel polymers designed specifically for each application can be cumbersome and expensive, blending macromolecules with well-known properties offers an attractive approach. Polymer blends add up to over one third of the annual total polymer consumption, and their significance is further increasing; there are thousands of patents filed every year. As polymer blends become more and more common, the amount of interfaces also escalates and the related phenomena pose novel challenges related to adhesion, compatibility and wear[86].[85]

Polymer blends can be miscible or immiscible. A miscible polymer blend is homogeneous at the molecular scale and thermodynamically distinguished with a negative value of the Gibbs free energy (or free energy of mixing, FEM) in addition to a positive second derivative (see paragraph on Figure 4 below). The entropy of mixing is always positive; therefore the mixing enthalpy determines the FEM.[87] In practise, a blend is miscible if the component

domains correspond to the size of the macromolecular segments.[85] Even though the definition of the miscibility is unambiguous, verification is not always straightforward. Flory-Huggins theory utilises a lattice model. Its modifications, along with engineering approaches such as solubility parameters, are often used to assess the solubility and thermodynamic parameters of polymer blends, albeit assumptions limit the predictive capability.[86,88] Recently, a novel approach to evaluate polymer blend miscibility was developed by Higgins *et al.*[88]. Despite several developed theories, experimental verification after blending the components is still often needed.[85] An example of this is T_g determination: a miscible blend has only one T_g while an immiscible blend has separate T_g's characteristic of the blend components. The majority of the blends are immiscible and in these cases the phases separate unless compatibilisation is applied.

Phase separation is the spontaneous process where polymer blends segregate into distinct phases.[87] It occurs when the polymers are in a mobile state (above T_g or T_m). The tendency to segregate is high, to the extent that protonated and deuterated counterparts can separate.[89] The phases formed, even though discrete, always contain traces of the other polymer as well and this has been described as secondary phase separation.[90]

Figure 4 depicts the correlation of the FEM as a function of polymer volume fraction and the related phase diagram. Conventionally, phase diagrams are used to assess blend behaviour. The binodal curve (Figure 4, bottom: solid black line) shows the limits of the miscibility region and is established from the common tangent points to the FEM graph, *i.e.*, where the chemical potential of the two phases is identical. In the metastable region between the binodal and spinodal curves (explained below), the initiation of phase separation happens *via* nucleation and growth (Figure 5, left top). Metastable materials can exist in a single phase for prolonged times.[91] The spinodal curve (Figure 4, bottom: solid, grey line) defines the limits of the metastable region of the system. It occurs at the tangent sign reversal and where the second derivative of the FEM is zero. The system is unstable to all concentration fluctuations inside the spinodal curve leading to phase separation *via* spinodal decomposition or, in the case of thin films, surface-directed spinodal decomposition (Figure 5, left bottom). The fully developed process would produce very large regions of two separate phases; then again, the spinodal architecture can be vitrified by cooling the mixture below its T_g.

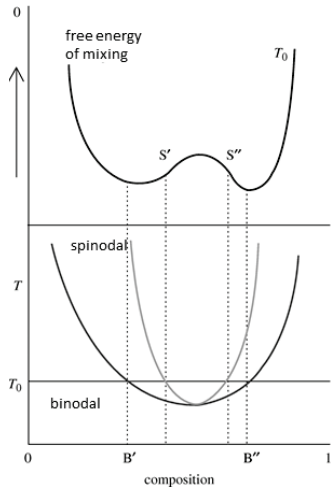

Figure 4. The Gibbs FEM as a function of polymer volume fraction at a chosen temperature T_o (top). The corresponding phase diagram shows the binodal (dark grey) and spinodal (light grey) boundaries; the binodal and spinodal compositions at T_o are denoted with B′ and B′′ along with S′, S′′ which are related to the features in the free energy curve (below).[88]

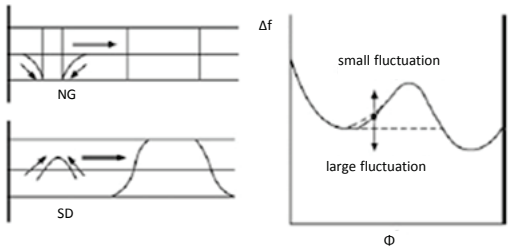

Figure 5. Concentration fluctuations under nucleation and growth (NG) and spinonal decomposition (SD) mechanisms for phase separation (left). Changes in FEM because of small and large fluctuations (right).[87]

The phase separation process in thin films prepared by solvent evaporation has been studied extensively, see, *e.g.*, Refs. 86 and 92. In most experimental investigations, phase separation occurs during the fast transition in temperature, *i.e.*, the quench. For weakly incompatible polymer blends it is feasible to define a Gibb's free energy at each point during the phase separation, but for intensely incompatible blends, this method is not valid. All the intrinsic parameters of the experimental system change constantly in an unknown fashion. As the diffusion kinetics of the solvent to the atmosphere is not known, it is not possible to explain the phase separation process in terms of the free energy model.[93]

2.5 Dewetting

Dewetting involves break-up of a thin film and it can be exploited when creating various architectures on film surfaces. Thin polymer films are utilised extensively in industrial processing and manufacturing. Understanding and controlling the stability and defect formation is vitally important.[94] Thick films stabilise *via* gravity. When the film thickness is below the capillary length ($\lambda_{,cap}$), molecular forces dominate and film dewets, provided it is not stable. The capillary length is defined as,

$$\lambda_{cap} = \sqrt{\frac{\sigma_{lv}}{\rho g}}, \qquad (2)$$

where σ_{lv} is the liquid/vapour surface tension, and ρ is the density of the solution. When a droplet is placed on top of a surface two competing phenomena occur; the droplet spreading is energetically favourable due to interactions between the substrate and the drop, while the increased contact area simultaneously increases the surface energy between the two. The film is unstable according to the Young's equation[95] and dewets if surface tension dominates and a drop of liquid of molten polymer exhibits a 180° contact angle (CA) on a substrate (Figure 6). Young equation is expressed as,

$$cos\theta_Y = \frac{\gamma_{sv} - \gamma_{sl}}{\gamma_{lv}}, \qquad (3)$$

where θ_Y is Young's CA, γ_{sv} and γ_{sl} are the solid/vapour and solid/liquid interfacial free energies; and γ_{lv} is the liquid/vapour surface tension.[96]

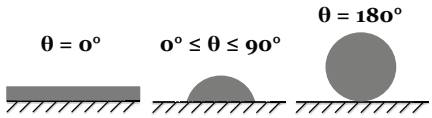

Figure 6. Various conformations of a liquid drop on a solid substrate: complete wetting (left), partial wetting (middle) and nonwetting (right). Adapted from Ref. 96.

The effective interfacial potential (EIP) of the air/film/substrate structure controls the dewetting for unstable films. The EIP represents the excess free energy per unit area necessary to bring two interfaces together from infinity. The distance between the solid/liquid and liquid/vapour interfaces is, in this case, the film thickness (h). Figure 7 presents three common dewetting scenarios. The dotted line defines an infinitely stable film; decreasing the

thickness from infinity (from right to left), energy is needed to thin the film. The bimodal and spinodal lines have a global minimum at film thickness $h=h_{equil}$ which means that the system can gain energy by shifting from any other given thickness to h_{equil}. The solid spinodal line and the dashed bimodal line delimit the border of the unstable and metastable film regions, respectively.[96]

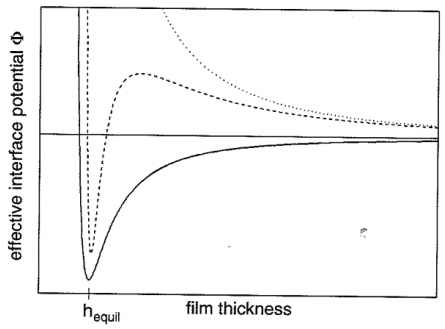

Figure 7. The EIP as a function of film thickness. The dotted line depicts a stable film, the dashed line a metastable film and the solid line an unstable film.[96]

Dewetting is depicted in Figure 8. It is usually initiated by annealing the film above T_g.[97] The process begins with film rupture, *i.e.*, hole formation, and proceeds with material transport from the hole site to the retreating rim (hole growth). Eventually, holes merge with the neighbouring holes to form polygonal ribbon-like features.[98] Ultimately, the ribbons coalesce into droplets due to capillary/Rayleigh instability.[96,99,100] Dewetting can be used for patterning since the structures mimic the morphology of the substrate.[44,101]

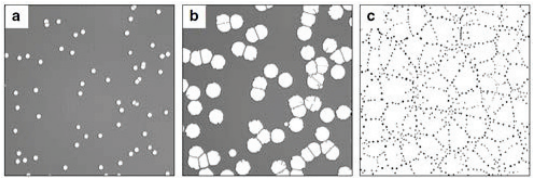

Figure 8. The dewetting process: a) film rupture, b) hole growth and c) droplet formation.[96]

The initiation of film rupture occurs either *via* nucleation or spinodal dewetting. Film rupture *via* nucleation is further divided into heterogeneous or homogeneous nucleation. When the film is metastable, an energy barrier has to be climbed to reach the potential minimum (dashed line, Figure 7). In heterogeneous nucleation, a nucleus, for example a dust particle, lowers the EIP facilitating dewetting; in homogeneous nucleation, however, thermal

activation overcomes the energy barrier. Homogeneous nucleation takes place close to the sign reversal of the second derivative of the EIP. Holes formed by nucleation are randomly distributed, in contrast to spinodal dewetting.[96]

Spinodal dewetting is a spontaneous film rupture mechanism which takes place when long-range molecular forces do not favour wetting. Thermal fluctuations induce exponentially growing surface undulations on an unstable film. Dewetting occurs when the amplitude reaches the film thickness.[102] The holes formed are periodically aligned: the length scale of the rupture correlates with the undulation wavelength that grows the fastest.[103] If the long-range forces are van der Waals forces, this critical wavelength (λ_c), scales theoretically to the film thickness: $\lambda_c \propto h^2$. The dewetting pattern is anticipated to behave correspondingly and if it is further assumed that every valley in an undulation forms a hole, the number density of holes (ρ), scales as $\rho \propto h^{-4}$.[98]

2.6 Morphology formation in thin blend films during spin coating

The polymer blend thin film is a system constrained between a free surface (towards air) and an interface (towards the substrate); the structure and kinetics of phase separation are, therefore, very different from the bulk.[7,104] The interplay between phase separation and dewetting during spin coating of blend films is complex and leads to various morphologies.[86,91,105] Although it has been studied to a great extent, full consensus of morphology formation does not yet exist.[105]

Walheim and co-workers state that film morphology is dictated by *i*) the different solubilities of the polymers in the common solvent; and *ii*) the varying substrate preferences of the polymers.[91] If the common solvent is a better solvent for the polymer that has lower surface tension, the topographical surface structure exhibits pointed edges and in the opposite case, round structures are detected (Figure 9). These results contradict the model by Tanaka *et al.*[106]. They are of the opinion that incomplete wetting of the substrate by the component with lower surface tension forces the other component to protrude from the substrate surface. Ton-That[107] *et al.* state that after vertical stratification, partial dewetting takes place.

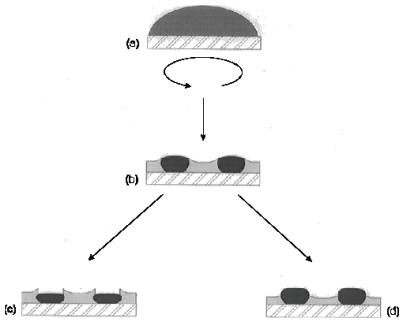

Figure 9. A model describing the morphology formation according to Walheim et al.. The shape of the domains is determined by the different surface tensions: the phase with the lower surface tension (dark grey) has a convex curvature (middle), as opposed to a concave structure on the other phase (lighter grey). As the solvent evaporates, one of the phases is depleted of the solvent before the other and the phase with better solubility collapses below the other layer. When darker or lighter phase has better solubility either sharp edges (left) or more round morphology (right) appears, respectively. Reprinted with permission from Ref. 91. Copyright (1997) American Chemical Society.

Experimental investigation of the evolution of film morphology is challenging and facilities suitable for this kind of research are rather scarce; however, some accounts exist. Heriot and Jones[105] along with colleagues[108] studied spin-coating of a binary polymer blend with time-resolved small-angle light scattering and light reflectivity. They gathered evidence that in the beginning of spin coating, the blend undergoes vertical stratification and subsequently, the interface between the layers becomes unstable, leading to the final, horizontally phase-separated film morphology. This theory is known as transient bilayer theory (Figure 10).

Recently, Ebbens and colleagues observed the morphology formation optically in binary blend films during spin coating and their hypothesis is depicted in Figure 11.[90] In films with final thickness in the range of *circa* 200 nm, they claim that phase separated morphology evolves well in advance, before polymer vitrification and that it does not undergo significant lateral stratification. Features that are present in the final morphology are visible when the film is thicker than two micrometres (few seconds before vitrification).[90]

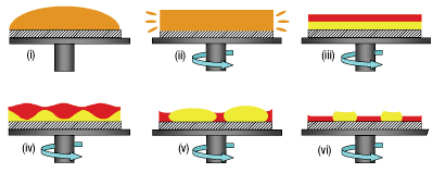

Figure 10. A model describing the transient bilayer theory: i) and ii) at the initial spin-off stage both polymer and solvent are removed. Next iii), the film separates into two layers and the film thins due to evaporation. Subsequently, iv) the layer structure becomes unstable and v) phases separate horizontally; and finally vi) the film solidifies. Reprinted by permission from Macmillan Publishers Ltd: Nature Materials, Ref. 105, copyright (2005).

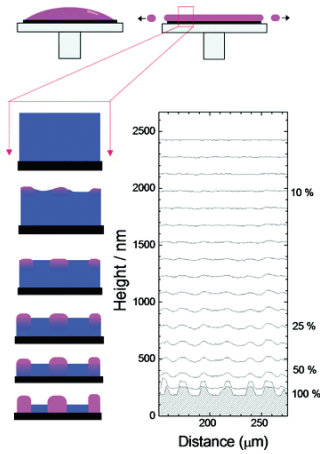

Figure 11. A cross-section of the phase separation process (left) and a quantitative surface topography at 0.25 s intervals (right); the estimated polymer content is stated right. Reprinted with permission from Ref. 90. Copyright (2001) American Chemical Society.

In summary, various factors play a vital role in morphology formation during spin coating. Such parameters arise from the individual polymers (M_w,[109] solubility,[91] surface tension[91] and viscosity), the blend solution (component ratio[27,110] solid content[111] and solvent properties[91,93]) and the substrate (roughness[96] and chemistry[44]) in addition to variations in ambient conditions (humidity[93]).

2.7 Non-woven fibre mats

The field of non-woven materials combines both mature and modern technologies and it has expanded from a limited amount into a vast mixture of materials, methods and applications.[112] An unambiguous description of non-wovens remains to be formulated, although there is a recent attempt to create a globally acknowledged definition (ISO standard 9092:2011). The broad

definition is they are textiles manufactured by untraditional means and made of fibres bonded together by fibre-fibre entanglement, mechanical treatment, heat, or chemical methods.[113] As is the case with knitted fabrics, every process has its unique qualities. Manufacturing steps from raw material selection, web formation, consolidation, and finishing can be used to tailor fabric properties.[112] The products have little in common aside being categorized as non-wovens. Because of the immense assortment of characteristics, the applications of non-woven fibre mats range from transportation, electronics, packaging, and filtration to hygiene and medical markets.[114] The preparation of non-wovens, electrospinning, and electrospun polysaccharides are topics covered in the following paragraphs.

2.7.1 Preparation

Common techniques for the ultrathin non-woven polymer fibre mat production, in addition to electrospinning, are melt blowing and multicomponent processes.[115] These methods exploit thermoplastic polymers and they produce fibres with diameters smaller than 500 nm. In short, melt blowing is a continuous one-step process where polymeric resin melts are extruded through an array of nozzles and drawn with high velocity air to form filaments deposited onto a conveyor.[116] Multicomponent fibres contain fragments of the chosen polymers which are prepared by extrusion techniques, *e.g.*, by means of water jets. Even though both of the aforementioned techniques have higher productivity than electrospinning, the benefit of electrospinning is better control of fibre morphology. Electrospinning offers the ability to construct various nano- and microscaled architectures.[117]

Electrospinning

The first patent describing electrospinning was filed in the 1930s,[118] but it took half a century for the process to start gaining wider attention.[119] Currently, electrospinning is a common technique, applied both in academia and in industry to manufacture polymeric nano- and microfibres from solutions or melts. There are several extensive reviews on electrospinning;[117,120-123] therefore, only a concise introduction is given here. The process is rather straightforward, versatile and it produces continuous fibres, a challenging task to achieve using other methods. The basic electrospinning setup includes three parts: a source of high voltage, a spinneret and an earthed collector (Figure

12). At first, electrospinning may seem misleadingly simple; however, it can be a rather intricate process as it depends on a multitude of parameters (Table 2).

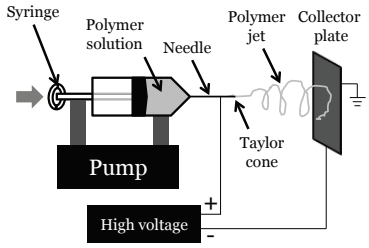

Figure 12. The setup for horizontal electrospinning. Adapted from Ref. 124.

Table 2. The parameters that determine the formation and structure of the electrospun fibres. Adapted from Refs. 119 and 125.

Solution	Process	Environment
Concentration, viscosity and viscoelasticity	Voltage	Temperature
Polymer solubility, molecular weight, Mw and Mw distribution	Tip-collector distance	Relative humidity (RH)
Polymer Tg	Flow rate	Air flow in the spinning cabinet
Solvent vapour pressure	Capillary geometry	
Surface tension	Collector type	
Conductivity		

The applied high voltage triggers a cone-shaped deformation, known as Taylor cone,[126] on the drop of the polymer solution in the direction of the collector (counter electrode). When the electrical potential at the tip of a spinneret exceeds the threshold value of the polymer solution surface tension, a polymer jet is produced. The solvent evaporates while the charged jet travels and bends in the electric field to the earthed collector, forming a non-woven fibre network.[119] During evaporation the surface charge density of the fibre increases, leading to an increase in repulsion between the fibre segments. The jet undergoes a whipping or a bending instability – long wave perturbations of a polymer jet, deriving from the electrostatic interactions between the surface charge and the external field.[124] The whipping instability can be understood if one considers a simple linear arrangement of three equal charges arranged on an elastic chain which becomes unstable towards lateral deflection.[127] A straight segment of the chain turns sideways and forms loops with increasing diameters as the chain moves through the electric field. This process is repeated until the fibre solidifies or becomes thin enough to resist the instabilities. Undesired beading of the fibre is caused by axis-symmetrical

instability – fluctuations in the radius of the jet trigger a surface charge density modulation which, in turn, generates tangential forces coupling and magnifying the radius modulation.[117] Electrospinning has been exploited in, *e.g.*, filtration[128] and biomedical applications[129].[114]

2.7.2 Electrospun cellulose and cellulose derivatives

The electrospinning of cellulose has been studied to a limited extent probably due to the same limitation as with ultrathin films – the difficulties in cellulose dissolution. The first patent on electrospinning[118] described the formation of CellA and propionyl cellulose fibres and since then, some studies on electrospun cellulose, both dissolved directly[130-132] and *via* derivatives,[33,118,133] have been published. Analogous to thin film preparation, the utilisation of direct solvents requires additional treatments to fully remove all traces of the solvent systems; thus, cellulose derivatives offer a simplified route for fibre mat preparation. CellA has gained plenty of attention and the subsequent regeneration of the CellA fibre mats has been explored.[125,134] Other electrospun derivatives include carboxymethylated,[135] hydroxypropylated,[135] methylated,[135] ethylated;[136] and propionylated[118,136] cellulose. CellA blended with poly(vinyl alcohol)[137] and carboxymethyl cellulose composites with polyethylene oxide[135] have also been electrospun to enhance the quality or properties of the fibres.

3. EXPERIMENTAL

The main polymers utilised in this work are presented in the Materials section. The applied characterization methods and some theory behind the main techniques are presented in the Methods section.

3.1 Materials

3.1.1 Trimethylsilyl cellulose and cellulose triacetate

In **Papers I-III**, TMSC was synthesized and characterized as described previously.[50,138] In short, the preparation of TMSC began with the activation of cellulose *via* solvent exchange and dissolution according to McCormick *et al.*[66] The synthesis was accomplished with hexamethyldisilazane. After subsequent recrystallisation, filtration and methanol wash, the TMSC yield was dried, ground and characterised. The purity of the synthesis product was confirmed with IR.

The weight average molecular weight and the number average molecular weight of TMSC were *circa* 2.31 × 10^5 and 8.3 × 10^4 g mol^{-1}, respectively, leading to a polydispersity index of 2.8. The DS according to XPS was ~2.1. In the work related to **Paper IV,** TMSC was obtained from Thuringian Institute of Textile and Plastics Research. According to the manufacturer, the DS of TMSC was 2.8. The hydrolysis procedure of TMSC to cellulose is explained in detail below.

CTA was obtained from Fluka. The acetyl content was 43–49 wt % which corresponds to a DS of ~3. The hydrolysis of CTA is also discussed in detail below. The chemical structures of TMSC, CTA and cellulose are shown in Chart 1.

Cellulose R=H

Trimethylsilyl cellulose R=Si(CH_3)$_3$

Cellulose triacetate R=COCH$_3$

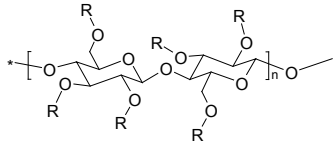

*Chart 1. Chemical structure of cellulose, TMSC and CTA. (**Paper III**)*

3.1.2 Other materials

Substrates - Silicon wafers (Si 100 with a native oxide layer on top, Okmetic, Vantaa, Finland) cut to *circa* 1 x 1 cm^2 pieces were utilised as supports for the ultrathin films. Wafers were hydrophilised in the UV ozonator for at least 15 min prior to use. Silicon dioxide crystal substrates for QCM-D studies were purchased from Q-Sense (Stockholm, Sweden). Aluminium foil was used as a support for the non-woven fibre mats. *Polystyrene* (PS) from Aldrich had a molecular weight of 280 kDa according to the manufacturer. The *water* used was of ultra-high quality purified by the Millipore Direct-Q® 3UV (Millipore, Molsheim, France). *Albumin from bovine serum (BSA)* (A7030) was purchased from Sigma-Aldrich and the purity was ≥98 % according to the manufacturer. The product was principally fatty acid and globulin free and M_w was *circa* 66 kDa. *Gold nanoparticles (AuNPs)* (741965) were obtained from Sigma-Aldrich and the diameter was 20 nm, PDI<0.2, core size 18-22 nm and mean hydrodynamic diameter 28-36 nm, according to the manufacturer. Poly(allylamine hydrocloride) (PAH, Aldrich) used for depositing a cationic layer on anionic AuNPs had M_w ~58 000. *All solvents and other chemicals* were of analytical grade and were used as obtained from the manufacturer.

3.2 Methods

In the following paragraphs, the theoretical background of the main techniques used in this work are presented (Scheme 2). An introduction to spin coating and electrospinning techniques used for film and fibre mat preparation was presented elsewhere in this thesis (Sections 2.3.1 and 2.7.1, respectively). AFM was used to study the surface morphology. Contact angle measurements (CAMs) gave information on surface energy. Surface chemistry was studied mainly with XPS and IR. The quartz crystal microbalance with dissipation monitoring (QCM-D) was used to characterise swelling, stability, adsorption and viscoelastic properties. An elaborated description of the experimental procedures can be found in the attached papers and the respective supplementary data sections.

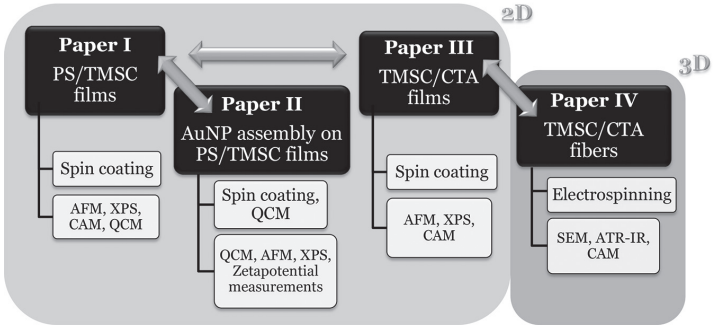

Scheme 2. A summary of the different characterization methods used in this work.

3.2.1 Film and fibre mat preparation

Ultrathin films of bicomponent blends were prepared with spin coating; fibre mats were prepared by electrospinning. These methods were presented Chapter 2.

Spin coating procedure. The blend components were dissolved separately to a concentration of 10 g dm^{-3}. Blends were prepared by mixing the two solutions and diluting with solvent so that the majority component concentration was 5 g dm^{-3} (**Papers I-III**). The pure cellulose film for the QCM-D studies was prepared from a 5 g dm^{-3} TMSC solution to obtain the same amount of cellulose as in the blends (**Papers I and II**). The spin coater utilised was the WS-650SX-6NPP/LITE (Laurell Technologies Corporation, North Wales, PA, USA). Prior to mounting the substrates on the spin coater, they were kept in the UV/ozonator for at least 20 min; the bare substrates were rinsed twice with the corresponding solvent (4000 rpm for 10-15 s) before spin coating with the polymer blend solutions. A drop of the blend solution was placed on the static substrate and then the spin coating was performed with a spinning speed of 4000 rpm and with an acceleration speed of 2130 rpm × s^{-1}. The spinning was continued until *circa* 30 s after the disappearance of the Newtonian rings which typically took place during acceleration with the systems used in this work.

For spin coating under low-humidity conditions (RH ≈ 15%), the spin coater chamber was carefully dried and flushed with nitrogen before mounting the substrate. For spin coating under higher humidity, water at different temperatures was introduced to the spinning chamber. The RH was monitored

in situ with a testo 625 probe (Brandt Instruments, Prairieville, LA) above the substrate. (**Paper III**)

Regeneration or hydrolysis of TMSC to cellulose. The spin-coated TMSC containing films were hydrolysed, *i.e.*, converted to cellulose in a 10 wt % aqueous hydrochloric acid vapour environment for 2 min (Scheme 3). The bulky structure due to trimethylsilyl groups is compressed to a tightly packed, hydrogen bonded structure typical of cellulose. The film thickness decreases approximately to one third of the initial value, which is in accordance with several other studies[26,50,81]. The cellulose obtained is amorphous[138] and the PS domains are not affected by regeneration. No washing steps were required to obtain pure cellulose films after regeneration. (**Papers I-III**). An identical approach was used for fibre mats in **Paper IV**.

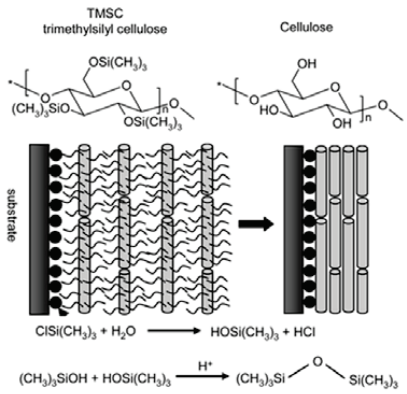

Scheme 3. The hydrolysis of TMSC to cellulose. The reactions at the bottom describe the by-product reactions; trimethylsilylchloride is instantly hydrolysed to trimethylsilanol which in turn condenses into hexamethyldisiloxane.[139] The volatile hexamethyldisiloxane diffuses through the film. Reproduced from Ref. 15 with permission of The Royal Society of Chemistry.

Regeneration or hydrolysis of CTA to cellulose. The fibre mats containing CTA were regenerated to cellulose in a 14 wt % aqueous ammonia vapour atmosphere, a procedure modified from Kasai and Kondo[70]. For full conversion of CTA, the fibre mats were kept in a desiccator with ammonia vapour atmosphere for 11 days. Due to such a long regeneration time, some condensation of the ammonia solution on the mats was noted. Thus, after the regeneration, fibre mats were rinsed with ultra-purified water (**Paper IV**).

A detailed schematic on various possible modification paths for TMSC and CTA containing bicomponent systems is shown below (Scheme 4, **Papers III**

and **IV**). A similar approach was also used for the PS/TMSC systems, only with the exception that the PS phase was left intact (**Papers I** and **II**).

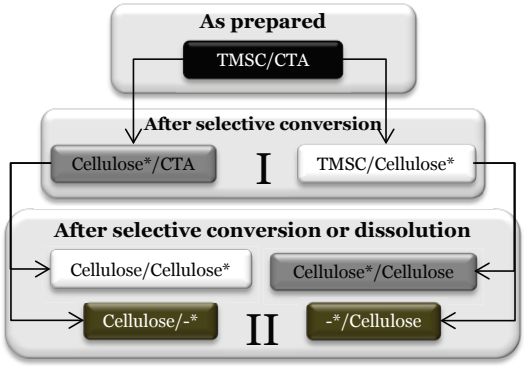

*Scheme 4. The potential modification routes for a TMSC/CTA blend system. Adapted from **Paper IV**.*

Electrospinning procedure. The horizontal setup consisted of a computer-controlled syringe pump (Aldrich) to inject the polymer solution through a needle (d = 1.37 mm) connected to the positive terminal of a high-voltage supply unit (Series EL, Glassman High Voltage). A metal plate (d = 30 cm) covered with aluminium foil was used as a earthed collector connected to the negative electrode of the power supply. The electrospinning parameters were selected by performing a series of test runs.

3.2.2 Atomic force microscopy

Scanning probe microscopy (SPM) originates from the beginning of 1980s, when Heinrich Rohrer and Gerd Binnig invented scanning tunnelling microscopy.[140] SPM denotes a family of techniques which uses a physical probe to scan the surface and they differ from optical microscopy because they exploit the interaction between the surface and the probe to generate an image of the surface rather than visualising it directly. AFM is part of the SPM family and after its invention and commercialisation in the 1980s it has become an indispensable tool for materials and nanoscience by virtue of minimal sample preparation, ambient operating conditions and reasonable price.[141]

The AFM principle is shown in Figure 13. A sharp tip connected to a cantilever scans the sample surface by means of piezoelectric controller. The vertical movements of the tip due to surface topography cause deflections on the cantilever; the deflections are recorded from a reflected laser beam. In theory,

topographical information down to single atoms could be obtained if the tip would be sharp enough. In practice, it is only possible under special circumstances,[142] because the common radius of curvature is in the range of 5-10 nm. The small area of the tip in contact with the imaged surface leads to a repulsive force at the contact area due to overlapping electron shells of the tip and surface atoms (Figure 14). In addition, long-range forces (*e.g.*, dipole–dipole interactions, van der Waals dispersion forces and capillary forces due to a humidity induced water layer between the tip and the surface) exist and they can be either attractive or repulsive.[143]

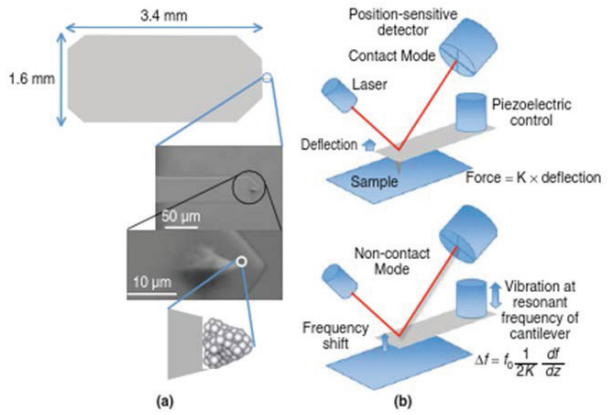

Figure 13. Principle of AFM-imaging. The cantilever and tip are shown on left and the two main operating modes are depicted on right.[5]

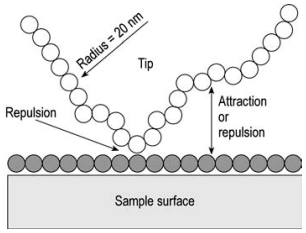

Figure 14. Forces as the probe scans in the vicinity of the surface. Blank and grey circles represent the atoms in the probe and sample, respectively. Copyright Wiley-VCH Verlag GmbH & Co. KGaA. Reproduced with permission.[143]

AFM has two main operating modes – contact and dynamic. Dynamic intermittent contact mode (tapping or alternating current mode) is most relevant for deformable polymeric samples. The cantilever is oscillated near or at its resonance frequency and the changes in oscillation amplitude are monitored. Despite AFM's many advances and positive effects on materials science, some limitations exists in its imaging capability. The tip apex

geometry defines the lateral precision, and errors in interpretation can occur if sufficient caution is not taken. The vertical precision on the other hand is high. Also, occasionally, a small fragment of sample may adhere to the tip causing deformations to the film and in the image.

AFM Imaging procedure. Film surface morphology and layer thickness was determined using the Nanoscope IIIa Multimode scanning probe microscope (Digital Instruments Inc., Santa Barbara, CA, USA). The images were scanned in tapping mode with a J-scanner and silicon cantilevers (NSC15/AIBS from Ultrasharp, μ-Masch, Tallinn, Estonia). The radius of curvature for the tip according to the manufacturer was less than 10 nm and the typical resonance frequency of the cantilever was 325 kHz. Two parallel surfaces were prepared and at least two areas on each were imaged. No image processing besides flattening was performed. All quantitative data were extracted from the height images. The film thickness was studied by scratching the samples with a needle and determining the height difference between the exposed substrate and the intact areas of the film.

Image analysis was performed using Nanoscope (version V6.13 R1, Digital Instruments Inc., Santa Barbara, CA, USA), Nanoscope Analysis (version 1.20, Veeco, Plainview, NY, USA) and Scanning Probe Image Processor (SPIP) (version 4.5.3, Image Metrology, Lyngby, Denmark) software. The pore surface coverage was determined using the Grain Analysis module in SPIP with the Threshold algorithm.

3.2.3 Contact angle measurements

Phenomena related to CAMs were briefly discussed earlier in Section 2.5. In the bulk, molecules are pulled equally in every direction by adjacent molecules which leads to a net force of zero. The molecules at the surface, however, are pulled inward by the adjacent molecules. Thus, the liquid spontaneously contracts its surface area to reach the lowest surface free energy (Figure 15).[144] The CA (θ) is defined at the three-phase contact line, *i.e.*, the angle that forms at the intersection of the liquid-solid and the liquid-vapour interfaces (Figure 16); it can be determined with Young's equation (Equation 3, page 15). CAs smaller than 90° designate that wetting and thus the consequent spreading of the liquid is favoured, while CAs above 90° indicate unfavourable wetting leading to formation of a compact liquid droplet. In the case of water as the probe liquid, the former are called hydrophilic and the latter hydrophobic.

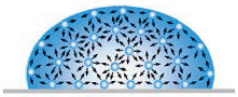

Figure 15. The surface tension is caused by the unbalanced forces of liquid molecules at the surface. Adapted from Ref. 144.

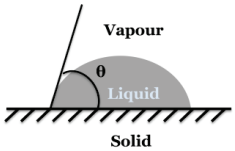

Figure 16. Partial wetting of a solid by a liquid.

The surfaces under scrutiny are assumed to be ideal: homogeneous, smooth, rigid, and inert to the probe liquids. Additionally the CA is considered characteristic for a given solid-liquid system in certain conditions[145]. Experimental surfaces, however, seldom meet the criteria set by Young's equation. Wenzel developed a model for rough surfaces:[146]

$$cos\theta_W = r\,cos\,\theta_Y, \qquad (4)$$

where r is roughness factor which is determined as the ratio of the actual to the nominal surface area. Roughness enhances both hydrophilicity and hydrophobicity. Cassie-Baxter studied heterogeneous wetting:[147]

$$cos\theta_{CB} = \phi_A cos\theta_A + \phi_B cos\theta_B, \qquad (5)$$

where θ_{CB} is the CA, ϕ_A and ϕ_B are the coverage of the components A and B, and θ_A and θ_B the CAs of the individual components. The previous equations are stated to be correct only when the drop is large in comparison to the roughness.[148] The Wenzel model is based on complete liquid penetration into indentations as opposed to the Cassie–Baxter approach; where air pockets below the drop and inside the indentations are also considered (Figure 17).[149] The Wenzel state surfaces are predicted to be "sticky" while the Cassie–Baxter state is characteristic for "slippy" surfaces.[150,151] In addition to conventional Wenzel and Cassie–Baxter models, *e.g.*, Wang and Jiang have proposed several modified hydrophobic states.[152]

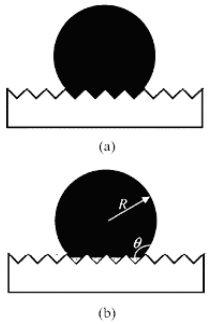

Figure 17. A drop of water on a hydrophobic, rough surface: a) homogeneous (Wenzel) and b) heterogeneous (Cassie-Baxter) wetting scenario. Reprinted with permission from Ref. 149. Copyright (2003) American Chemical Society.

Static CA has been considered a random metastable state in between the dynamic, *i.e.*, advancing and receding CAs.[153-155] However, most authors agree that they can be exploited in assessing relative surface characteristics. The use of dynamic CAs evades the ambiguity of the static CAs. Contact angle hysteresis (CAH) is the difference between the advancing and the receding angle and it arises either from chemical or topographical surface heterogeneities.[153,156]

CAM procedure. CAMs with water were performed with the CAM-200 contact angle goniometer (KSV Instruments Ltd, Helsinki, Finland) in ambient air at room temperature. Static equilibrium CAs were determined at the three-phase line when stable values were observed (less than 10 s after drop deposition). The dynamic CAs were obtained by slowly (0.1 μdm^{-3} s^{-1}) increasing and decreasing the volume of a small water droplet. At least five measurements from two different surfaces per test point were performed. CA calculations were performed with the CAM-200 software (KSV Instruments Ltd, Helsinki, Finland). The calculations are based on a numerical solution of the full Young–Laplace equation.

3.2.4 X-ray photoelectron spectroscopy

XPS has been applied in the field of cellulose research since the late 1970s.[157] The basis of the technique is the photoelectric effect: the emission of electrons upon energy ($h\nu$) absorption from x-ray irradiation (Figure 18, left). XPS measures the emitted electron kinetic energy which can be used to calculate its binding energy, which in turn depends on the atom the electron originates from:

$$E_k = h\upsilon - E_b - \varphi, \qquad (6)$$

where E_k is the kinetic energy of the electron, h is Planck's constant, υ is the frequency of the exciting radiation, E_b is the binding energy of the photoelectron and φ is the instrument specific work function. Simultaneously with the photoelectric effect, another phenomenon occurs. The vacant place left by the photoelectron is filled with a relaxing higher shell electron. The energy released is taken up by another electron, called the Auger electron, which is again emitted with an element-specific kinetic energy (Figure 18, right). Moreover, the XPS can be utilised to characterise chemical states, *i.e.*, various chemical bonds in, *e.g.*, carbon.[158]

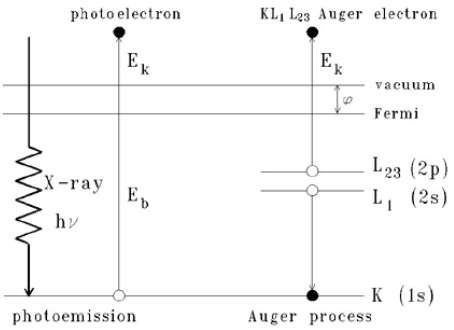

Figure 18. The photoelectric (left) and Auger (right) processes.[159]

The main experimental restriction of the XPS is the ultra-high vacuum conditions needed. Also, sample preparation is sensitive to contamination that can arise from vacuum pump oil in the instrument itself. The quantitative treatise is somewhat challenging; a homogenous surface distribution is needed to obtain unbiased results. A nuisance, especially in organic samples, is heterogeneous charging.

XPS procedure. The chemistry of the film surfaces was studied with XPS. The measurements were performed with an AXIS 165 (Kratos Analytical, Manchester, UK) spectrometer using a monochromated Al Kα x-ray source. All samples were pre-evacuated overnight to stabilize the ultra-high vacuum (UHV) conditions. The UHV condition was monitored thorough the measurement. Two parallel samples were prepared and each sample was analysed at least at three points. The elemental surface composition was determined from low resolution scans recorded with 80 eV pass energy and 1 eV steps. Carbon 1s and oxygen 1s high resolution spectra were determined

using 20 eV pass energy at 0.1 eV steps. The carbon 1s emission was resolved into various contributions corresponding to distinct chemical states of carbon according to the literature.

3.2.5 Quartz crystal microbalance with dissipation monitoring

QCM-D in essence is a highly sensitive scale. It was developed for and it is exploited commonly in adsorption studies. A quartz crystal is oscillated at its fundamental resonance frequency and changes in frequency and dissipation of the crystal are determined with the resonance frequency and its overtones.[160] The benefit of conducting experiments with several overtones is the analysis of possible vertical variations in the adsorbed layer. The adsorbed mass depends on the decrease in frequency according to Sauerbrey equation:[161,162]

$$\Delta m = -\frac{C\Delta f}{n}, \qquad (7)$$

where C is the device sensitivity constant (17.7 ng Hz^{-1} cm^{-2} for a 5 MHz quartz crystal), f is the fundamental resonance frequency and n is the overtone number. The adsorbed mass inherently contains a contribution from bound water as well. The assumptions in Sauerbrey equation are that the adsorbed layer is rigidly bound and evenly distributed; in addition, the adsorbed mass should be small compared to the mass of the crystal.

Dissipation offers information on the frictional losses due to the viscoelastic properties of the adsorbed layer. The dissipation is determined by turning off the driving voltage and monitoring the amplitude decay. Rigid layers are characterised with low dissipation energies (short damping periods) while highly viscous layers exhibit high dissipation energies owing to frictional losses. The dissipation is defined as:

$$D = \frac{E_{diss}}{2\pi E_{stored}}, \qquad (8)$$

where E_{diss} is the dissipated energy during one oscillation and E_{stored} is the total energy stored in the oscillation system.

For viscous films, the Sauerbrey equation underestimates the adsorbed amount. A model by Johannssman *et al.* has been proposed to better estimate the mass instead:[163]

$$\hat{m}^* = m^0 \left(1 + \hat{J}(f) \frac{f^2 \rho d^2}{3}\right), \qquad (9)$$

where $\hat{m}^*$ is the equivalent mass; m^o is the true, sensed mass; $\hat{\hat{J}}$(f) is the complex shear assumed independent of the frequency; f is the resonance frequency in liquid and, ρ is the density of the fluid and d the thickness of the film. The true sensed mass can be determined from the intercept of the curve where the equivalent mass is depicted as a function of square of its resonance frequency.

The Voigt-based model (parallel spring and damper) provided by Q-Tools analysis software can also be used to estimate the adsorbed amounts. This iterative approach utilises frequency and dissipation data from several overtones.[164] The well-tried fitting parameters from Orelma *et al.* were applied.[165]

QCM-D procedure. Studies were conducted with a Q-Sense E4 instrument (Q-Sense AB, Gothenburg, Sweden). The cellulose containing films were stabilised overnight in their respective buffers prior to measurements. The constant liquid flow during the measurements was 0.1 mdm-3 min-1. All measurements were recorded at the 5 MHz fundamental resonance frequency and its overtones at 15, 25, 35, 55, and 75 MHz. The third and fifth overtones were used in data evaluation. Each experiment was repeated at least twice.

3.2.6 Other methods

Scanning electron microscopy (SEM). The fibre mat and fibre surface morphology were investigated using a JSM-6400F microscope (JEOL Ltd., Tokyo, Japan) operated at an accelerating voltage of 5 kV and a working distance of 20 mm. Prior to the imaging, a *circa* 25 mm² piece of the mat was fixed on conductive carbon tape, mounted on the support and sputtered with a ~6 nm layer of gold/palladium.

Attenuated total reflectance infrared (ATR-IR). The chemistry of the fibre mats was analysed with the Bio-Rad FTS 6000 spectrometer (Cambridge, MA, USA) equipped with a diamond internal reflection element. A constant mirror velocity of 20 Hz, a 5 kHz filter, and an 8 cm^{-1} resolution was used to scan the 4000–700 cm^{-1} wavelength region. Air background spectra were gathered before each set of measurements. A minimum of 200 scans per spectrum were collected, ATR-corrected and normalised at 1300 cm^{-1}. The spectra shown in

Paper IV are averages of at least three measurements from various points of the fibre mat.

The specific surface area of the selected fibre mats was determined by *nitrogen adsorption–desorption measurements* with the Omnisorp 100CX (Coulter, Miami, FL, USA) at liquid nitrogen temperature. The sample was dried at hundred degrees for ten hours prior to the measurements. Both adsorption and desorption isotherms were measured and the surface area was determined from the adsorption curve by the Brunauer–Emmett–Teller (BET) method.

Differential scanning calorimetry (DSC) measurements were done with DSC Q100 (TA Instruments, New Castle, DE, USA). The heating–cooling cycle between 25–250 °C was repeated twice using a heating rate of 10 °C min^{-1}. These measurements gave information on the polymer thermal behaviour and, more specifically, on T_g.

A confocal Leica DMRXE microscope (Leica Microsystems GmbH, Mannheim, Germany) was used in the analysis of the fibre mat roughness. The roughness was determined from 750×750 μm^2 images collected from several points of the sample.

Photoacoustic infrared spectroscopy was performed with the Bio-Rad FTS 6000 spectrometer (Cambridge, MA, USA) with the Gasera PA301 photoacoustic cell (Turku, Finland) and *size exclusion chromatography* (Waters, Milford, MA, USA) was utilised in TMSC characterization after the synthesis step (**Papers I-III**).

Zeta potential measurements (Zetasizer Nano series, Malvern Instruments Ltd, Worcestershire, UK) were used to verify the AuNP modifications in **Paper II**.

4. ULTRATHIN FILMS

The results presented in this chapter originate from **Papers I-III.** The section on PS/TMSC films is based on **Paper I** and **Paper II** while the section on TMSC/CTA films comes from **Paper III**.

4.1 Polystyrene/trimethylsilyl cellulose films

The aim of this work was to introduce a method to prepare reproducible cellulose films of tunable functionality. More specifically, the goal was to create a template for NP immobilisation. This was achieved by blending TMSC with PS and spin coating the mixture into an ultrathin film. In general, a simple method to quantitatively tailor the surface morphology and chemistry of ultrathin cellulose films in a single step during the film preparation was presented (**Paper I**). To demonstrate the feasibility of the films developed as an NP immobilisation template, a straightforward method to assemble AuNPs on the flat PS/TMSC or PS/cellulose blend films with micro- and nanoscale lateral precision was shown in **Paper II**.

4.1.1 Morphology

Spin coated immiscible polymer blend films create systematic patterns by virtue of limitations triggered by the interfaces.[92,104] Typically, the architectures formed are micronsized,[27,36,86,91,166] however, when the concentration of the minority phase is small enough nanosized domains emerge.[107,110,167,168] Also, utilisation of block copolymers results in nanosized architectures.[169] The quench during toluene evaporation during spin coating PS/TMSC films resulted in smooth, laterally phase separated morphologies with nanosized round and disk-like PS domains (Figure 19). The convex shape of the PS discs and the circular cross-section of PS features originated from the surface tension difference and significant immiscibility with TMSC (Figure 20).[91] During the regeneration of TMSC to cellulose, protruding PS domains (height *circa* 5–20 nm) appeared. Furthermore, the films were stable in aqueous environment for extended periods of time, and only the cellulose matrix had an effect on the swelling of the blend films.

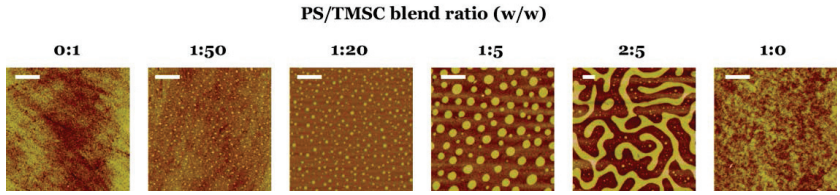

Figure 19. Representative AFM height images of a series of PS/cellulose films. The scale bar correspond to 1 µm. The PS/TMSC blend ratios (w/w) in the original spin coating solutions are stated on top. The blend ratio 0:1 refers to cellulose and the ratio 1:0 to PS surfaces. Adapted from ***Electronic Supplementary Information of Paper II****.*

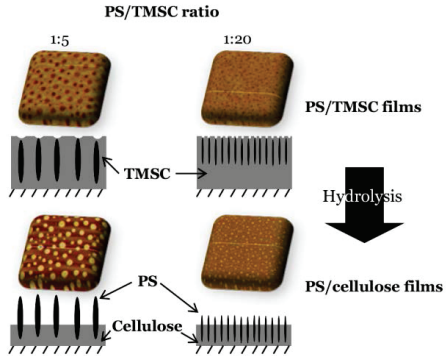

Figure 20. Cross-sectional schematics of the blend films. PS/TMSC films (top): the blend ratios 1:5 (left) and 1:20 (right) and the corresponding films where TMSC is hydrolysed to cellulose (bottom). The respective representative AFM height images are on top of each schematic. In the AFM height image of the PS/cellulose film, the light PS domains are higher while dark areas rich in cellulose are lower. The dimensions are not to scale; the vertical direction is exaggerated significantly in comparison to the horizontal one. Adapted from ***Paper I****.*

The film morphology in the spin-coated polymer blend films was dictated by consecutive phase separation and dewetting. At the initial stage of the spin coating, PS and TMSC segregated vertically (Scheme 5). TMSC is less hydrophopic compared to PS which leads to its preferred enrichment on the hydrophilic SiO_x substrate; thus the PS layer accumulated at the polymer/air interface. The upper PS layer became unstable and broke due to dewetting. Finally, the PS-rich phase coalesced into droplets. The morphology formation followed the well-known transient bilayer theory (see Section 2.6).[105] To confirm that dewetting was the reason behind morphology formation, the films were annealed above the T_g of PS for 24 hours and indeed, no additional dewetting occurred.[105,168]

Scheme 5. The morphology formation of PS/TMSC films via transient bilayer theory. Adapted from ***Paper I****.*

When the film thickness, the PS coverage, and the PS domain height were extracted from the AFM height images, the film morphology could be quantified and the volume of each component in the film was calculated. The calculations are shown in the Supporting Information of **Paper I**. The correlation between the PS/TMSC ratio in the initial spin coating solution and the PS/cellulose ratio in the films is illustrated in Figure 21. The discrepancy between these ratios was explained in part by the fact that the PS/TMSC is a mass ratio while that for the PS/cellulose is a volumetric one. Regeneration of TMSC to cellulose had an effect as well. The complementary quantification of the effect of the blend ratio in the films was done with XPS and the measurements are in agreement with the AFM results. The higher the PS/TMSC ratio in the initial spin coating solution, the higher the amount of PS in the films. The results also correlate with other studies of polymer blend thin films.[166-168] It was concluded that the initial blend ratio can be utilised to linearly tailor the blend composition in the obtained cellulose/PS films. Also, the dimensions of the PS domains varied linearly on the amount of PS in the original spin-coating solution: the less PS in the solution, the smaller the PS domains in the films.

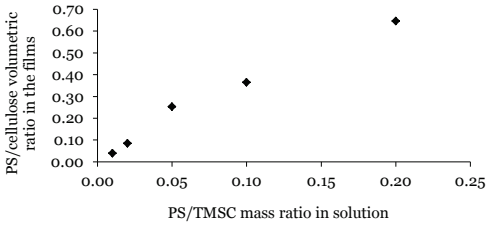

*Figure 21. The linear correlation of the volumetric ratio of PS and cellulose in the films with the mass ratio of PS and TMSC in the original spin coating solution. The volumes of the component are calculated based on the data extracted from AFM height images. (****Paper I****)*

4.1.2 Tunable hydrophobicity

Pure cellulose films hydrolysed from TMSC were hydrophilic (WCA 59±1°) and PS films hydrophobic (WCA 91±2°), therefore the bicomponent films are inherently characterised with tunable hydrophobicity. This characteristic can be regarded as an additional asset for the versatile template system. Since the ratio of the blend components in the films depends linearly on the ratio in the original spin-coating solution (Section 4.1.1), the solution polymer ratio could be used to tailor the wetting properties of the films. Thus, when the amount of hydrophobic PS in the spin coating solution increased, the WCA also increased. The WCA of the PS/cellulose films increased from 61° to 71° when the relative amount of PS was increased from 1:100 to 1:5. The 10° difference in WCA seemed unexpectedly subtle compared to the rather drastic difference in the PS amount. Hence, the experimental CAs were compared to those calculated from the Cassie–Baxter equation. The equation has its limitations,[154,170] but it offers a tool to estimate the CAs of bicomponent films. The experimental CAs coincided rather well with the calculated ones.

The WCA of cellulose regenerated from TMSC seemed surprisingly high compared to literature values (ranging from 25° to 49°).[26,74,171,172] However, the WCAs reported in these articles are from films prepared with the LB technique that results in more crystalline films compared to those from spin coating.[138,172] The theoretical wetting limit (equilibrium WCA) determined by molecular dynamic simulations for cellulose I_β was 43°.[173] Yamane *et al.* have reported a correlation between surface wettability and orientation of $(1^{-}10)$ crystal planes and crystallinity.[174] They found that the more crystalline the film was, the lower the WCA. Recently, a few accounts on CAs of spin coated cellulose films regenerated from TMSC were published and the WCA was in the range of 25-33°.[78,175] The main difference compared to this work was that the regeneration procedure was performed without vacuum; also, the M_w and DS of the TMSC utilised differed.

Additionally, the effect of consecutive wetting and drying of the blend films on WCA was studied. The history of the films proved to be important, because cellulosic materials go through irreversible changes upon wetting and subsequent drying.[176] The WCAs on pure cellulose films decreased *circa* 20° after a wetting-drying cycle, while the WCAs on the blend films decreased approximately 10°.

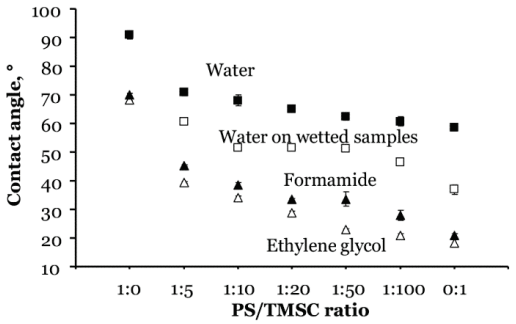

*Figure 22. Static WCAs on PS/cellulose films: with water ■, water on wetted samples □, formamide ▲, and ethylene glycol △. Angles are the average, the error bars represent the standard deviation from all the measured parallel samples. (**Paper I**)*

4.1.3 Gold nanoparticle immobilisation

Even though the morphology and tailorable properties of the PS/TMSC films are intriguing, to further explore the possibilities of the obtained blend films developed in **Paper I**, NP immobilisation on the films was carried out (**Paper II**). Combining the hierarchical film morphology with metal NPs can lead to tunable optical properties and electrical and thermal conductivity with corresponding applications in optics[177] and electronics[178]. The method created exploits the combination of three simple and well-known physico-chemical phenomena: *i)* phase separation of immiscible polymer blends, *ii)* site-specific adsorption of BSA protein on PS domains on an ultrathin cellulose film; and *iii)* the electrostatically driven adsorption of AuNPs on BSA (Scheme 6).

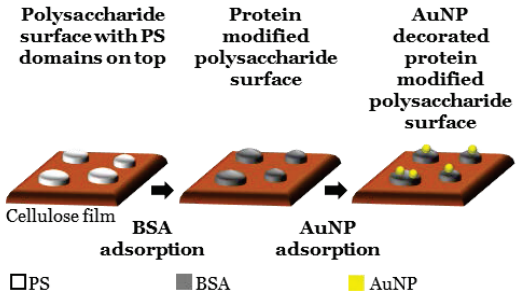

*Scheme 6. Schematic representation of the protein-assisted 2D assembly of AuNPs. The dimensions are not drawn to scale: the vertical dimensions are exaggerated compared to the horizontal one. (**Paper II**)*

Adsorption can be described as a process in which matter moves to and accumulates at the interface. The prerequisite for adsorption is that the interaction between adsorbate and the surface has to be stronger than the

interaction between the solvent and the adsorbate. Adsorption can involve either formation of chemical bonds between surface ions or atoms on the solid and the polymer molecules or weak physical interactions.[179] The PS/cellulose films developed offer an intrinsic opportunity for specific adsorption due to the alternating PS and cellulose domains. BSA protein is known to adsorb on PS while it is also known that cellulose hinders protein adsorption.[165,180,181] Proteins are an attractive platform for electrostatically driven adsorption due to their zwitterionic nature. Their charge can be tailored from anionic to cationic and *vice versa* by merely adjusting the pH. The isoelectric point (pI) of BSA is *circa* pH 5, below which the protein is cationic and above which it is anionic. Thus, the assembly of anionic and cationic AuNPs was performed below and above the pI, *i.e.*, at pH 4.5, and 7.5, respectively. The selective protein and AuNP adsorption studies were subsequently performed in, and confirmed with, a QCM-D device. In QCM-D, the decreasing frequency indicates increased adsorption or swelling of the adsorbed layer. The change in frequency (Δf) as a function of time during anionic AuNP assembly is shown in Figure 23.

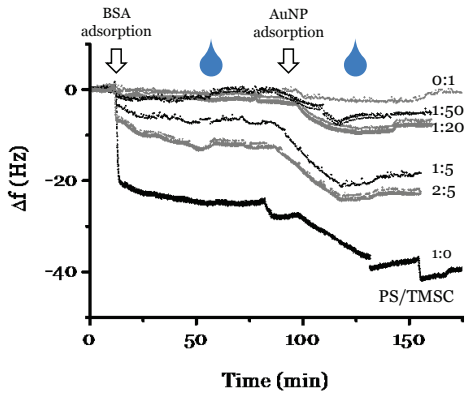

*Figure 23. The assembly of anionic AuNPs followed with QCM-D. The droplet indicates the time when rinsing (buffer and water) begun. PS/TMSC blend ratios (w/w) in the original spin coating solutions are stated left. The blend ratio 0:1 refers to cellulose and the ratio 1:0 to PS surfaces. (**Paper II**)*

The morphology of the films prior to the AuNP assembly was scrutinised both quantitatively and qualitatively in **Paper I** (Section 4.1.1). The film morphology after the selective assembly of the NPs was verified with AFM here as well. The structures decorated with AuNPs ranged from cellular network structures (Figure 24, e)) to discrete circular patches of variable sizes on cellulose surfaces (Figure 24, b)-d)).

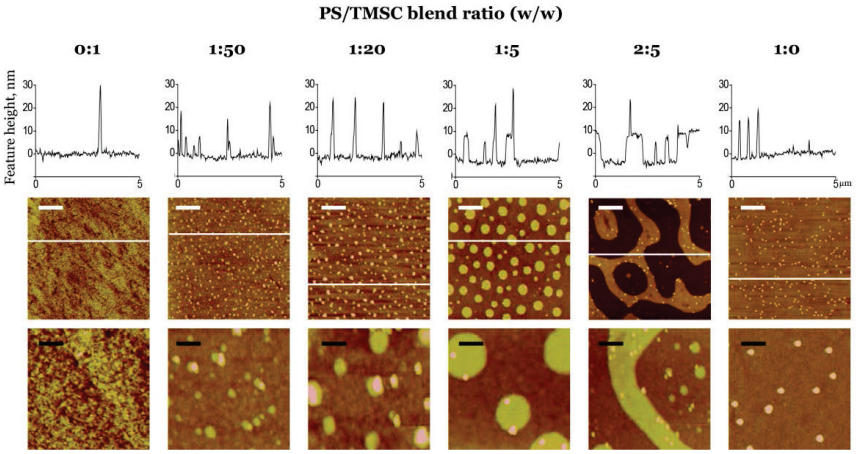

Figure 24. Representative AFM height images after AuNP assembly as well as individual height scans from the images after assembly (in the corresponding image, the white line indicates the place where the height scan is taken). The white and black scale bars correspond to 1 µm and 200 nm, respectively. The PS/TMSC blend ratios (w/w) in the original spin coating solutions are stated on top. The blend ratio 0:1 refers to cellulose and the ratio 1:0 to PS surfaces. Adapted from ***Electronic Supplementary Information of Paper II****.*

The quantitative analyses of attached anionic AuNPs from QCM-D, AFM and XPS experiments are in good agreement (Figure 25). The amount of PS dominated the AuNP adsorption process: the AuNP amount adsorbed increased with increasing proportion of PS in the films. The adsorbed amount of AuNPs is governed also by, *e.g.*, ionic strength, concentration, charge density of both the substrate and the NPs, and temperature. Here, their effect on the adsorption was not studied. However, when the measurement parameters and conditions were kept constant, the amount of PS controlled the amount of adsorbed AuNPs. The adsorption of cationic AuNPs was characterised and similar results were obtained.

To conclude, the PS/TMSC films developed show potential in many applications ranging from model films[15] to charge transport applications[178]. In addition, this NP immobilisation method could be further exploited due to the universal nature of the utilized phenomena. A variety of systems are feasible in principle: *i*) both cationic and anionic NPs can be utilised (demonstrated in **Paper II**); *ii*) as some 2D structures can be converted to 3D systems, an analogous method could be used to fabricate multicomponent 3D frameworks from cellulose and other polysaccharides coupled with different nano-objects and; *iii*) utilisation of click-activated or modified proteins could open new paths to engineered polysaccharide surfaces.[23]

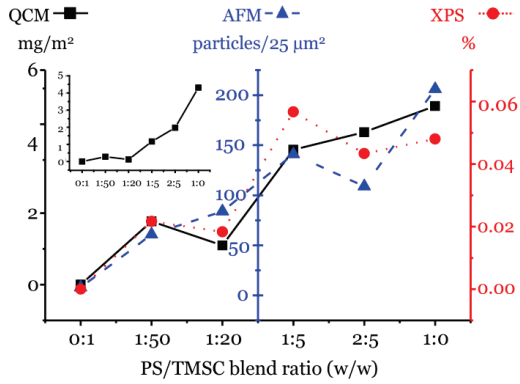

*Figure 25. Quantitative information of the anionic AuNP adsorption extracted from QCM (■, solid line), AFM (▲, dashed line) and XPS measurements (●, dotted line). The lines are added to guide the eye. Inset shows the results of the preceding BSA adsorption. PS/TMSC blend ratios (w/w) in the original spin coating solutions are stated on top. Blend ratio 0:1 refers to cellulose and ratio 1:0 to PS surface. (**Paper II**)*

4.2 Trimethylsilyl cellulose/cellulose triacetate films

Paper III focused on the construction of ultrathin bicomponent polysaccharide films with phase-specific pore formation. A hypothesis of the reasons behind the genesis and evolution of morphology was presented. This study follows in the footsteps of **Paper I** by utilising a bicomponent polymer blend to form ultrathin films; however, here the films were created by spin coating blends of two cellulose derivatives, namely CTA and TMSC, under varying humidity conditions. The formations of the morphologies obtained were tentatively assigned to vertical and lateral polymer phase separation, additional dewetting under humid atmosphere, and layer inversion during dewetting.

4.2.1 The effect of humidity

Jaczewska *et al.* have reported that varying water uptake by different polymer rich phases play a significant role in morphology formation when spin coating polymer blends under high humidity.[182] The effect of humidity during spin coating on the bicomponent thin film morphology was investigated with four relative humidity (RH) values and three TMSC/CTA blend ratios as well as pure TMSC and CTA films (TMSC/CTA 1:0, 10:1, 2:1, 1:10 and 0:1). Representative AFM height images of these films prepared under ambient air of low (~15 %), medium (~45 %) and high (~75 and ~95 %) RH are shown in

Figure 26. AFM exposed the nano- and microscale architectures that formed during spin coating blends of TMSC and CTA in chloroform. Based on Figure 26, it is obvious that humidity playes an important role in film evolution along with the blend ratio. Films obtained from pure TMSC and CTA were smooth and featureless when the ambient air during spin coating was of low or medium RH. When the components were blended at different ratios and spin coated, various morphologies emerged owing to changes in RH and polymer immiscibility leading to phase separation. All the blend ratios underwent pore formation when spin coating was carried out at the highest ambient air humidity. In the blend ratio TMSC/CTA 1:10, the pores appeared already at the ~75 % RH, in contrast to the behaviour observed for, *e.g.*, the symmetrical blend ratio TMSC/CTA 10:1. The CTA rich phase seemed to be more affected by the humidity. Also, the pore formation was enhanced when the amount of CTA in the films was in the given critical concentration range, namely, between 17-83 %. Medium humidity (~45 % RH) was chosen for additional experiments not only because this humidity is common in ambient conditions but also because of the diversity of the topographies formed on the surface of the films.

Pore formation under high RH atmosphere and a slow evaporation rate is commonly attributed to the breath figure formation, which will be discussed later.[183] Hecht and co-workers have ascribed porous morphologies in spin coated ultrathin films prepared under high RH to dewetting.[184] This is in contrast to work by, *e.g.*, Madej *et al.*[185] and Park *et al.*,[186] who claimed that the spin coating process proceeds too rapidly for the substrate to cool down enough for breath figure formation to occur. In addition to the abovementioned reasons, porous structures formed during spin coating have also been assigned to water incorporated in solvent.[83,185]

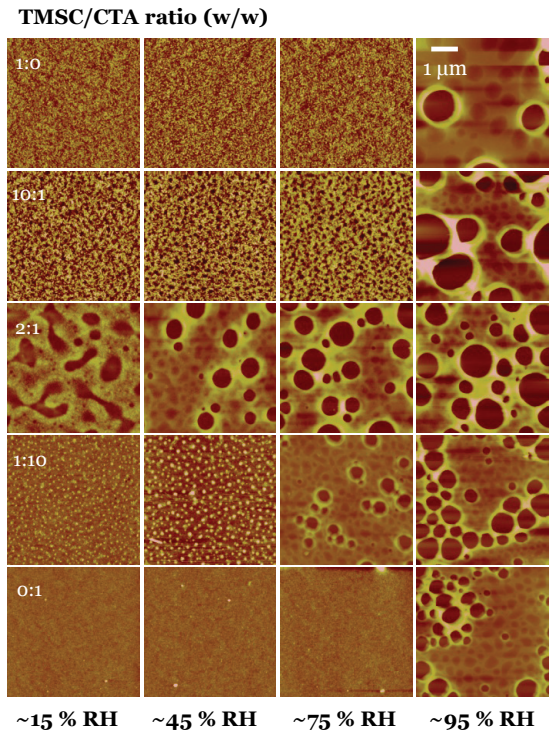

*Figure 26. Representative 25 µm² AFM height images portraying the effect of ambient RH during spin coating on TMSC/CTA blend films. (**Paper III**)*

4.2.2 Morphology

Figure 27 shows blend films prepared at RH 45 % from TMSC/CTA blends with mass ratios of 10:1, 5:1, 2:1, 1:2, 1:5 and 1:10. The films were imaged after spin coating and after the two following modification steps: *i*) selective hydrolysis of TMSC to cellulose caused vertical contraction of the TMSC-rich phase; and *ii*) a further selective dissolution of CTA phase enabled easier distinction of the blend components. Two sample sets could be recognised from Figure 27: films in excess of one component (TMSC/CTA 10:1 and 1:10) and intermediate blend ratio films (TMSC/CTA 5:1 – 1:5). In the former set, the morphology was distinguished by nanoscale domains on a continuous matrix, islands (TMSC/CTA 1:10) or valleys (TMSC/CTA 10:1), while the latter sample group was characterised by the formation of micronscale pores (TMSC/CTA 5:1 – 1:5). It is clear that two different phenomena, phase separation and pore formation, dictated the evolution of morphology in the blend films at RH 45%.

The regeneration to cellulose has an effect on morphology. However, the morphology formation is more influenced by the film deposition method. This was demonstrated, *e.g.* in the work of Aulin *et al.* who compared cellulose films regenerated from films prepared either by spin coating or LS technique.[172] An identical regeneration procedure was applied. Spin coated films were amorphous and LS-films were crystalline. It is probable that structural gradient, *i.e.*, inhomogeneity exists during the vapour phase regeneration process; however, once the regeneration is complete, cellulose forms a homogeneous layer. A neutron reflectivity study by Kontturi *et al.* showed that regenerated cellulose exists as homogeneous layer upon consecutive swelling and drying.[138] This indicates that regenerated cellulose films are free from structural gradients.

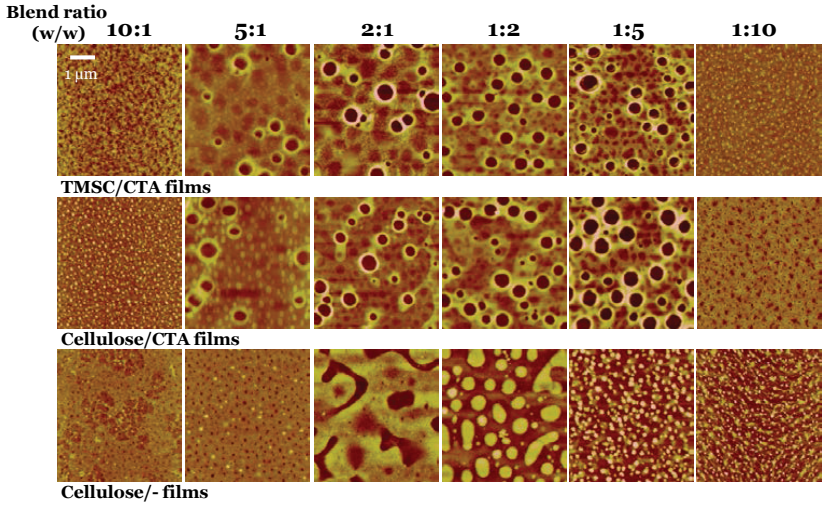

Figure 27. Representative 25 µm² AFM height images of the untreated TMSC/CTA films prepared at RH 45 % (top), cellulose/CTA films (TMSC converted to cellulose, middle), and cellulose/- films (TMSC conversion followed by a removal of CTA phase, bottom). ***(Paper III)***

Phase separation during spin coating immiscible polymer blends is a well-known phenomenon and it can be explained by transient bilayer theory, explained above (Sections 2.6 and 4.1.1).[105] The morphology of the blend ratios TMSC/CTA 10:1 and 1:10 can be understood by this theory. As for the intermediate blend ratios (TMSC/CTA 5:1 – 1:5), transient bilayer theory alone cannot explain the morphology. An additional pore growth step takes place when films were prepared in humid atmosphere.

The phase rich in TMSC contracted during the conversion to cellulose; however, no changes after the conversion of TMSC to cellulose were detected on the films from the intermediate blend ratios (TMSC/CTA 5:1–1:5) (Figure 27, top and middle rows). Pores and the rims remained intact during the first modification step and they disappeared only when the CTA was dissolved (modification step *ii*)). Thus, it was concluded that the pores were concentrated on the CTA-rich phase. This was also supported by AFM image analysis: the pore surface density in the films from intermediate blend ratios increased with increasing CTA fraction in the initial spin coating solution. Additional information extracted from Figure 27 was that the films did not peel off during selective CTA dissolution. This indicates that TMSC is enriched on the substrate surface. To elaborate the reasons behind the film morphology formation, the films were also characterised by AFM thickness analysis, XPS and CAMs in addition to investigating the effect of humidity. Furthermore, the films were annealed under nitrogen atmosphere.

Figure 28 highlights the results from XPS measurements: the percentage of O–C=O bond emission (fingerprint for CTA, left) and the relative amount of silicon (fingerprint for TMSC, right) are shown as a function of the fraction of CTA in the initial spin coating solution. The XPS investigation confirmed that both lateral and horizontal phase separation occurred. Had the experimental points in Figure 28 been linearly correlated, the films would have undergone only vertical phase separation. Further, XPS revealed that there was a TMSC-rich phase on the substrate surface (Figure 28, right).

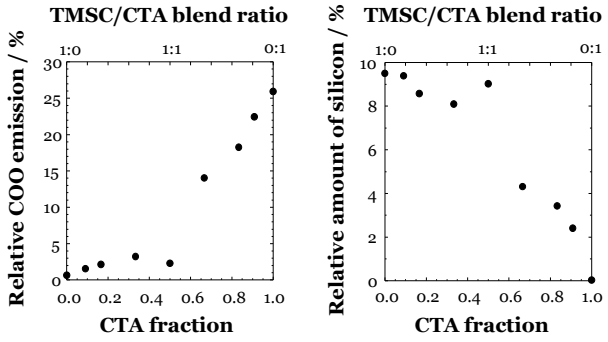

Figure 28. The percentage of carbon O–C=O bonds (left) and the relative amount of silicon (right) as a function of the CTA fraction in the original spin coating solution. The relative amount of the bond emission and relative atomic concentrations is obtained from the XPS measurements. Adapted from ***Paper III****.*

The most prominent CAM result was that even a small amount of TMSC was enough to bring the WCA close to WCA of pure TMSC (Table 3). This meant that in the blend films, TMSC formed a layer at the air interface as well as on the substrate surface. A tentative reason for the presence of the TMSC overlayer is layer inversion,[187,188] discussed further in the following section (4.2.3). An interesting result was also the observation that even though the film root mean square roughness varied between 0.3-31.9 nm, it had only a minor effect on the WCA. The differences between the apparent WCA and WCA for an ideally smooth surface calculated from Wenzel equation (Equation 4, page 30) were within the standard deviation (Table 3).

*Table 3. Experimentally measured apparent water contact angles (AWCA) and calculated CAs (CA_W). (**Electronic Supplementary Information of Paper III**)*

TMSC/CTA blend ratio	TMSC/CTA films		Cellulose/CTA films		Cellulose/- films	
	AWCA	CA_W	AWCA	CA_W	AWCA	CA_W
1:0 (TMSC)	93.3	93.3	58.6	58.6		
10:1	93.3	93.3	63.2	63.3	55.1	56.5
5:1	91.5	91.5	55.9	56.4	57.8	58.0
2:1	92.1	91.9	51.8	53.3	57.6	57.8
1:1	92.4	92.4	47.0	47.9	54.8	55.1
1:2	92.2	92.0	61.1	62.3	55.2	55.6
1:5	92.1	92.1	62.2	63.0	57.5	58.0
1:10	91.5	91.5	50.0	50.0	58.4	58.7
0:1 (CTA)	57.5	57.5				

4.2.3 Hypothesis on morphology formation

The experimental evidence gathered leads to the conclusion that several concurrent phenomena taking place upon spin coating were responsible for the evolution of the morphology in the films from intermediate blend ratios (TMSC/CTA 5:1–1:5). These are vertical and lateral phase separation, plasticization of the CTA phase under humid conditions, leading to additional dewetting and phase-specific pore growth and, finally, surface energy minimization *via* partial layer inversion during dewetting. As mentioned earlier, the transient bilayer theory explains the vertical and horizontal phase separation into TMSC-rich and CTA-rich phases (TMSC/CTA 10:1 and 1:10) (Scheme 7, left and right, three topmost images).[105] However, the observed additional pore formation needs more elucidation. The potential morphology formation paths for the films from intermediate blend ratios (TMSC/CTA 5:1–

TMSC/CTA 1:5) are depicted in Scheme 7: dewetting route (left) and breath figure formation (right).

Breath figures are indentations formed when slowly evaporating high vapour–pressure solvent cools the surface, enabling the condensation of water from the ambient air (Scheme 7, right). In contrast to the randomly distributed craters obtained here, breath figures are usually periodically aligned.[183] Furthermore, the rims around the pores are commonly absent from breath figures while they are typical for the pores formed by dewetting (Figure 29).[96] Also, the thin TMSC overlayer detected with CAM supports the dewetting scenario: several accounts show that during dewetting, the lower layer in a vertically phase separated film can replace the upper layer.[188-190] This phenomenon is known as layer inversion.

For polysaccharides, the T_g undergoes a reduction when exposed to water or water vapour.[191] For ultrathin films, T_g also reduces as a function of decreasing thickness.[192] In the TMSC/CTA films prepared under humid conditions, a plasticising effect due to humidity was assumed to occur and the reduced T_g of CTA hypothetically enabled an additional dewetting step. The plasticization of just CTA was likely because it is more hydrophilic when compared to TMSC (CAM). Also, the proposed presence of water at the interface between the blend components might have induced dewetting in a similar fashion to the dewetting of a spin coated polymer film on top of an unoriented water film.[184]

Finally, when a vertically phase-separated structure minimised its surface energy during dewetting, the material from the lower layer forms a continuous layer at the topmost surface.[188-190] Here, the dewetting CTA rim offers a potential layer inversion site and the CTA-rich phase penetrated in to the more mobile TMSC-rich layer. This in turn enabled part of the TMSC-rich phase to enrich at the air/film interface (Scheme 7, left). Bernasik and co-workers have stated that the segregation of the components can be suppressed in spin coated films prepared in a humid atmosphere.[193] Even though the favoured scenario is only a hypothesis, it offers a comprehensive explanation for the film formation process: vertical and horizontal phase separation according to the transient bilayer theory; pores surrounded by rims formed by an additional dewetting step, and finally the presence of a thin TMSC overlayer due to incomplete layer inversion taking place during the additional dewetting (Scheme 7, left).

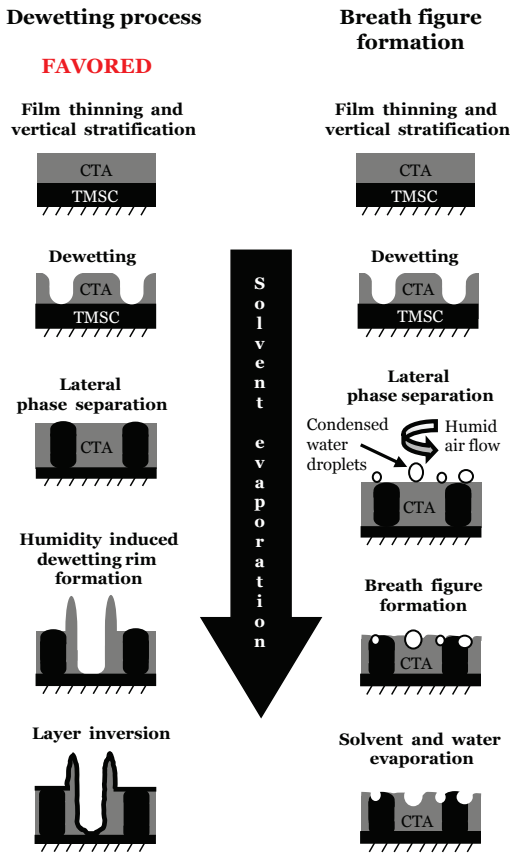

Scheme 7. Hypothetical processes to explain the morphology formation. The dimensions are not to scale, vertical dimensions are exaggerated compared to the horizontal ones. Adapted from ***Paper III****.*

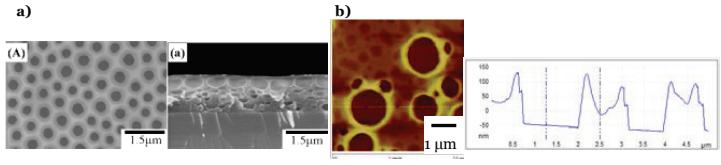

Figure 29. A comparison between pores formed by a) breath figure formation (SEM images) and b) dewetting (AFM height image). The SEM images were adapted with permission from Ref. 186. Copyright (1997) American Chemical Society.

4.3 On morphology formation of 2D films including cellulose derivatives

The choice of polymers and their properties has the most profound effect on morphology and the charactersitics of the film. The common feature in both PS/TMSC films (**Papers I and II**) and TMSC/CTA films (**Paper III**) was the

key role played by the blend ratio in defining morphology. It can be said that the initial polymer solution blend ratio dictates the morphology formation. In **Paper I** a linear correlation between the volumetric ratio of PS and cellulose in the films and the mass ratio of PS and TMSC in the original spin coating solution was established. The same could be assumed to be true for other films as well, however, in **Paper III**, this was not studied. External factors during spin coating, *e.g.*, ambient air humidity, play a vital role also. CTA domains in blend films in **Paper III** were greatly affected by humidity during the film preparation. The same effect was not noted in **Paper I**. This could be due to the more hydrophobic nature of the polymer blend components used in **Paper I**. However, after the TMSC regeneration the films are more susceptible to water or humidity which was demonstrated by the decrease in WCA (Figure 22). Similarly, for example, elevated temperatures during film preparation can be expected to affect the morphologies obtained. For supported ultrathin films, also the choice of a substrate can influence morphology, for instance, by preferential enrichment of one of the blend components. This work focused mainly on the effect of the blend ratio and humidity.

Concerning the paths to various morphologies, consecutive phase separation and dewetting taking place according to transient bilayer theory could be used to explain morphology formation for the films in **Paper I** and also the simplest cases in **Paper III** (the films from the blend ratios with excess of one component). The films prepared from the polymer solutions with middle blend ratios underwent an additional pore-growth step hypothesized to derive from plasticization of the CTA phase under humid conditions, and, additionally, surface energy minimization *via* partial layer inversion (**Paper III**). To conclude, some indication on common behaviour patterns could be noted, however, more research is needed to draw universal conclusions on morphology formation on ultrathin cellulose films.

5. NON-WOVEN FIBRE MATS

The results in this chapter are mainly based on **Paper IV**. As was the case in the previous papers, observing polymer blend behaviour was essential for this paper. The threads of this work have been the morphology formation (**Paper I** and **Paper III**) and modification (**Paper I** and **Paper II**) of ultrathin polymer blend films. Here, the polymer blend investigation was expanded to the field of non-woven fibre mats. The aim was to fabricate non-woven fibre mats with tailorable chemical composition and surface and wetting properties. Also, transferring the peculiar 2D TMSC/CTA film morphologies (from **Paper III**) into 3D fibre systems was attempted. Fibre networks were prepared by electrospinning the hydrophobised cellulose derivatives used in **Paper III**, TMSC and CTA, dissolved in a common solvent. Through conversion of the respective components to cellulose, the chemical and adsorption properties of the fibre networks were tuned without significantly altering the large-scale network morphology.

5.1 Morphology

SEM images obtained from the TMSC/CTA blend fibre mats (Figure 30, top) and larger magnification images of the individual fibre surfaces (Figure 30, bottom) are shown below. Previously, porosity has been introduced to electrospun fibre mats by utilising, for instance, extremely volatile solvents,[194-196] breath figures,[194] coaxial spinning[197] and cryogenic liquids.[198] Here, SEM revealed the formation of fibre mats with individual porous fibres. By varying the polymer blend ratio in the initial electrospinning solution, the following range of morphologies emerged: TMSC fibre mats that contained non-continuous micronscale fibres with shallow dints; TMSC/CTA 5:1 mats of flat micronscale fibres with regular pore arrays; TMSC/CTA 1:1 mats of wrinkled micronscale fibres decorated with superficial dints and occasional larger pores; TMSC/CTA 1:5 mats of flat micronscale fibres with ellipsoidal porous structures; and finally CTA mats with smooth micron- and submicronscale fibres. The morphology of the fibre mats obtained also contained defects; however, with careful optimisation of the electrospinning parameters, thinner and more uniform fibres could potentially be created. Formation of defects, *i.e.*, beading, has been explained by an axis-symmetric jet instability – instead of the thinning by asymmetrical whipping, the jet fluctuates around its main axis.[199] ATR-IR confirmed that the greater the amount of blend component in

the initial electrospinning solution, the higher the amount of the component in the fibre mat, an observation analogous to the blend films.

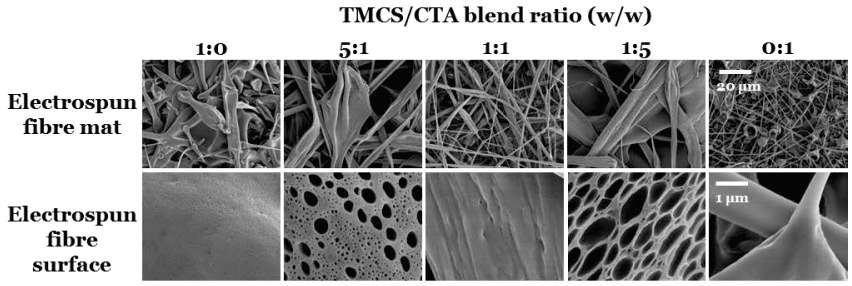

Figure 30. Representative SEM images of TMSC/CTA blend fibre mats (top) and respective fibre surfaces (bottom). The TMSC/CTA blend ratios are stated on top and the scale bars are on the right. Adapted from ***Paper IV*****.**

5.2 Ultrahydrophobicity

As mentioned earlier, TMSC is hydrophobic while CTA and cellulose are more hydrophilic, thus, a feature always linked to the hydrophobised cellulose derivative blend systems is the possibility to tailor the wetting properties. A comparison of the WCAs of the 3D fibre mats and 2D ultrathin films is shown in Table 4. The equilibrium WCAs in the flat films were between 93 ± 1° (pure TMSC) and 58 ± 0.5° (pure CTA). The respective WCAs for the fibre mats varied between 150 ± 11° (pure TMSC) and 129 ± 2° (pure CTA). Roughness is known to enhance hydrophobicity as well as hydrophilicity and that effect is significant for the fibre mats. CAMs also indicated that TMSC was enriched on the fibre surface, a result also obtained in the case of ultrathin films (**Paper III**).

*Table 4. A comparison of the static WCAs of TMSC/CTA 3D fibre mats and 2D ultrathin films. The WCAs of blend films are indicated in parenthesis. The modification of CTA-rich phase was studied in fibre mats only. (****Paper IV****)*

	Fibre mat WCA (film WCA), degrees				
TMSC/CTA blend ratio (w/w)	1:0	5:1	1:1	1:5	0:1
Untreated (TMSC/CTA)	150 ± 11 (93 ± 0)	152 ± 8 (92 ± 2)	136 ± 3 (92 ± 0)	139 ± 3 (92 ± 1)	129 ± 2 (58 ± 1)
TMSC converted (Cellulose/CTA)	0 (59 ± 1)	0 (62 ± 1)	0 (47 ± 1)	129 ± 3 (56 ± 2)	
CTA converted (TMSC/Cellulose)		142 ± 2	120 ± 5	130 ± 4	31 ± 5 (13 ± 2)

To avoid ambiguity in the CAM, the advancing and receding CA were also measured (Figure 31). The fibre mats had advancing WCAs in the range of *circa* 130-160 degrees. The most characteristic feature, however, was the high CAH, a minimum of 50 degrees. The pure CTA fibre mat had the largest CAH of approximately 140 degrees. Traditionally, two models are used to explain contact-angle behaviour on rough homogeneous surfaces: the Wenzel (homogeneous) model and the Cassie–Baxter (heterogeneous) model. The Wenzel state is described as adhesive to the probe liquid while the Cassie–Baxter state, on the other hand, as "slippy" (Figure 17).[150,151] It was observed here that water droplets stay adhered to the blend fibre mats, even when the mat was turned upside down. This behaviour indicates a Wenzel-type system. Similar behaviour was reported by Feng *et al.*, who named this hierarchical micro- and nanostructured morphology enabled hydrophobicity with high adhesive force to water as the petal effect.[200] Lubrication,[201] printing[202] and microfluidics,[203] have been suggested as potential applications for such systems. Hydrophobic structures have gained enormous attention since the first publication by Onda *et al.*[204] of wetting on fractal surfaces. At the same time, the terminology has expanded and Roach *et al.* proposed a consolidated terminology for high CA surfaces. For an increase of CA by roughness, they suggested the use of the following terms: *i*) "positive CA enhancement" for CAs<120°; *ii*) "ultrahydrophobicity" for CAs>120°; and *iii*) "superhydrophobicity" when the CA>150° is increased due to roughness and the CAH is less than ten degrees.[205]

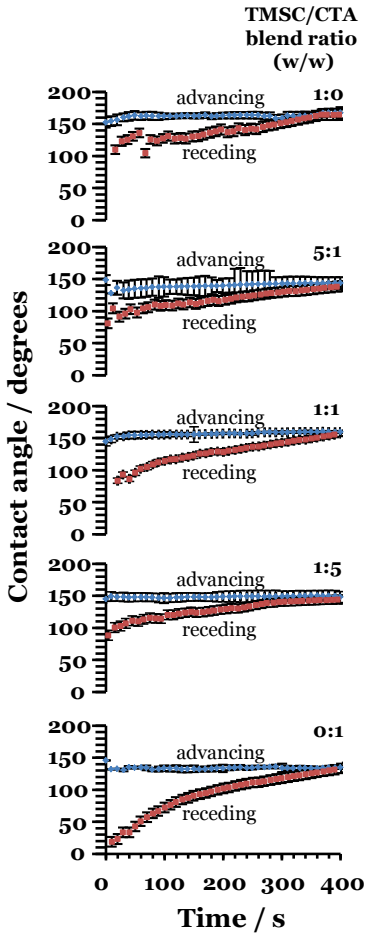

*Figure 31. Dynamic WCAs for untreated TMSC/CTA blend fibre mats. Angles are the average of at least three measurements and two separately-prepared mats, the error bars represent the standard deviation. (**Paper IV**)*

5.3 Fibre post-treatment

Ultimately, the selected fibre mats (TMSC/CTA 5:1) were subjected to the post-treatment steps presented in Scheme 4 (Section 3.2.1). The first modification was selective conversion: either of the two cellulose derivatives could be selectively converted to cellulose to obtain "TMSC/Cellulose" or "Cellulose/CTA". The second modification consisted of the following two paths: *i*) conversion of the remaining cellulose derivative to cellulose (producing "Cellulose/Cellulose"); or *ii*) selectively dissolving the non-converted cellulose derivative with chloroform (producing "Cellulose/-" or "-/Cellulose"). The component modified last is marked with an asterisk (*) in the

following paragraphs. The success of the post-treatments was investigated by ATR-IR (Figure 32).

Due to the selected blend ratio, 5:1, the TMSC contribution dominated the IR spectra. After subsequent selective TMSC regeneration and CTA dissolution ("Cellulose/-*"), the CTA contribution in the IR was still noticeable (Figure 32). It was assumed that CTA was enclosed by a cellulose layer (formerly TMSC) in the fibres, thus preventing solvent diffusion and therefore selective dissolution (Scheme 9). In addition to the IR results, this assumption was supported by the CAMs. Selective CTA conversion was observed to be effective ("TMSC/Cellulose*"), but sequential CTA and TMSC conversions ("Cellulose*/Cellulose") seemed incomplete (Figure 32). Also, the characteristic peaks of the dissolved component did not disappear after successive CTA conversion and TMSC dissolution ("-*/Cellulose"). This was also hypothesised to stem from the separation of the components inside the fibre: in addition to enriching on the fibres, TMSC was speculated to reside inside the cellulose (formerly CTA) matrix (Scheme 9). The diffusion of the component selective solvent inside the cellulose matrix was hindered, preventing both the TMSC regeneration and dissolution which would explain the incompletion of the discussed post-treatments leading to ("Cellulose*/Cellulose") and ("-*/Cellulose") fibre mats.

The effect of the post-treatments on the fibre mats and fibre surface morphology was also investigated with SEM (Figure 33). Also the WCAs are shown in Figure 33 to highlight the changes in surface chemistry. There were no visible changes in the large scale fibre mat morphology after the modification stages. Changes were apparent only after closer examination of the fibre surface. The pore dimensions seemed slightly distorted in the two cases with cellulose derivative conversion and sequential dissolution ("Cellulose/-*") and ("-*/Cellulose"). Possible explanation of the high WCA of the ("-*/Cellulose") fibre mat is the fact that during selective dissolution of a component from a polymer blend some re-adsorption of the polymer in question takes place.[206]

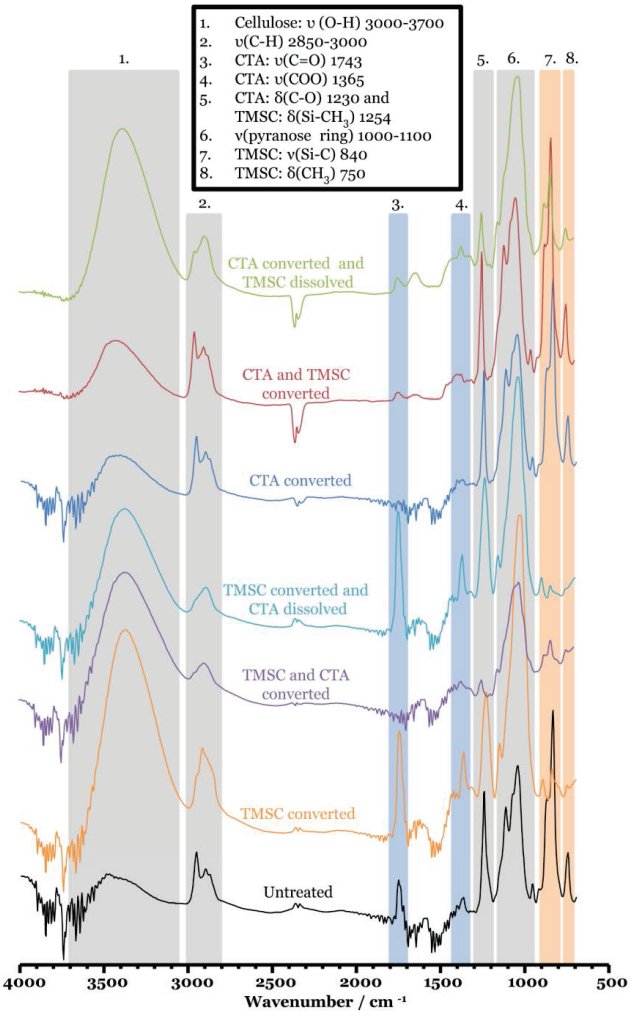

*Figure 32. IR spectra confirming the modifications performed on the TMSC/CTA 5:1 fibre mats. The characteristic peaks for TMSC (orange), CTA (blue) and cellulose (grey) are highlighted and explained in the legend. (**Paper IV**)*

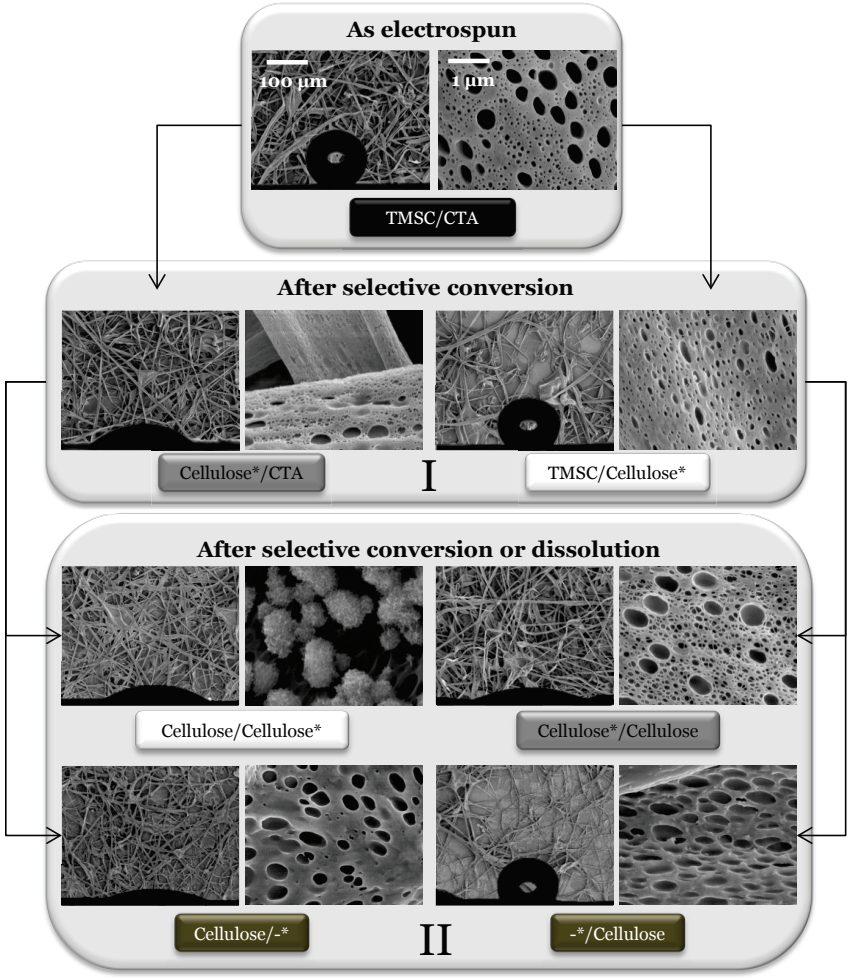

Figure 33. SEM and static equilibrium WCA images of the fibre mats prepared from TMSC/CTA 5:1 as prepared and after the post-treatments following Scheme 4. The first modification stage (I) indicates two possible modification paths: regeneration of either TMSC or CTA to cellulose. The second modification stage (II) is comprised of two possible modification paths: selective dissolution or conversion of the remaining component. The modified component is marked with an asterisk. The scale bars (100 µm, left and 1 µm, right) from the top carry on throughout the figure for each pair of SEM images. Adapted from ***Paper IV*****.**

5.4 Hypothesis on morphology formation

The porous structure in the blend fibres has been denoted to arise from the rapid phase separation during electrospinning.[195] Bognitzki *et al.*[198] have sketched potential fibre morphologies for fibres prepared from polymer blends (Scheme 8). Based on these and a careful summary of the experimental findings presented in the earlier paragraphs, a hypothetical schematic of the blend fibre was drafted (Scheme 9). However, the verification of the

hypothesis on morphology would require additional efforts. The proposed complementary techniques include mercury porosimetry or confocal microscopy for the determination of the size of macroscopic pores between the fibres, comprehensive AFM imaging to determine the roughness of single fibres, XPS investigation taking into account the determined roughness values to define the chemical composition of the fibre mats, and elemental analysis to quantify the remaining TMSC and CTA after regeneration and/or selective dissolution.

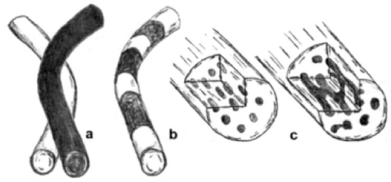

Scheme 8. The possible morphologies of bicomponent fibres according to Bognitzk. a) fibres consisting of the pure polymers, fibres composed of sequences of individual polymers, c) matrix-dispersed or co-continuous phase morphologies with dimensions smaller than the fibre diameter.[198]

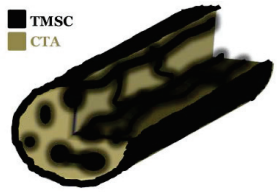

Scheme 9. A hypothetical fibre structure. Adapted from ***Paper IV*****.**

5.5 From 2D into 3D structures

One of the aims in this investigation was to convert the morphologies produced in 2D film structures (**Paper III**) into 3D fibre systems. Hypothetically, a similar approach could be applied to other polymer blend systems as well.

The SEM images of the blend fibre surfaces were compared to the AFM images of the blend films (Figure 34) and this offered the possibility to compare the 3D fibre surface morphologies to the morphologies of the 2D films prepared from the same polymer blend system. In general, the ratio of components in the initial polymer blend solution seems to govern the morphology in both 2D and 3D architectures (**Papers I-IV**). The surface morphologies of the blend fibres resembled rather closely the morphologies of the blend films. The pure

components produced rather smooth architectures – TMSC films and fibres were slightly rougher than the counterparts obtained from CTA. Both TMSC/CTA 5:1 mats and TMSC/CTA 1:5 mats had porous surface structures. Overall, similarities, but also some differences in 3D and 2D architectures are noted. Further research efforts are needed to produce more universal conclusions. However, the results indicate that the porous 2D film morphologies can be, at times, reproduced in 3D polymer blend fibre mats.

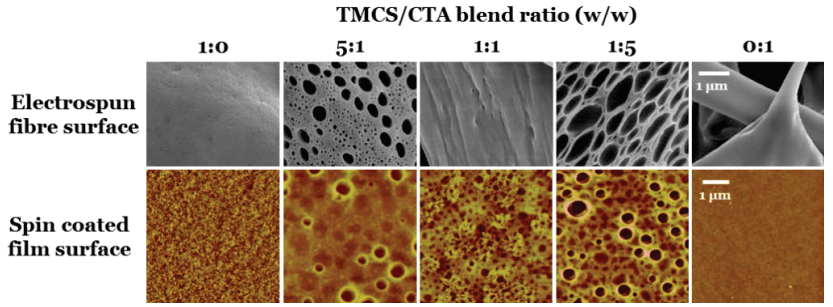

Figure 34. Representative SEM images of TMSC/CTA blend fibre surfaces (top). The AFM height images of the respective ultrathin TMSC/CTA blend films (bottom) are included for comparison. The TMSC/CTA blend ratios are stated on top and the scale bars are on the right. Adapted from ***Paper IV****.*

6. CONCLUDING REMARKS

Paper I focused on modification of ultrathin films from polymeric PS/TMSC blends. The surface chemistry and morphology of the films was scrutinised and quantified. The morphology of the films was tailored in a single step during film preparation, simply by adjusting the polymer blend composition in the initial spin coating solution. Hydrophobic functionalization was simultaneously achieved with this simple film preparation method. The PS/cellulose films were characterised by subtly tailorable hydrophobic properties, indicating promising potential to expand the range of existing cellulose films. Other polymers besides PS could be combined with TMSC to produce cellulose films with desired functionalities. **Paper II** explored a modification path for the films developed in **Paper I**. It combined the well-established phenomena of immiscible polymer blend phase separation, specific adsorption of BSA protein on PS patches on a cellulose film and electrostatic adsorption of AuNPs to the pre-adsorbed BSA. The AuNP assembly produced films with varying morphologies that spanned from cellular network structures to discrete circular patches on cellulose. The assembly process was quantified and the AuNP amount in the films increased with increasing proportion of PS in the films. Zwitterionic proteins offer an intriguing platform for electrostatic adsorption and, in this work, the adsorption of cationic AuNPs was performed as well.

Paper III studied the morphology formation of spin coated ultrathin polymer blend films with phase-specific pore formation. This study stemmed from **Paper I**; however, the polymers used were both of polysaccharide origin. A tentative hypothesis to explain the genesis and evolution of morphology was provided. The formation of the morphologies obtained was attributed to vertical and lateral polymer phase separation, an additional dewetting stage under humid atmosphere, and finally, layer inversion during dewetting. Other potential explanations are also described. In short, the first part of the thesis (**Papers I-III**) highlighted the vast potential of cellulose containing polymer blends to form various nano- and microscale architectures on ultrathin films.

Finally, **Paper IV** also investigated polymer blend behaviour, only this time concentrating on non-woven fibre mats. The exciting 2D TMSC/CTA film morphologies from **Paper III** were transferred into 3D fibre mat structures. In this study, electrospun fibre mats with tunable chemical composition and

surface and wetting properties were produced. The blend fibre mats obtained were porous and were characterised with high WCAs. Additionally, they displayed high CAH and water droplets stayed pinned on top of the fibre mats.

The work in this thesis was a fundamental endeavour to deepen understanding of various polymer blend architectures. It encompassed a set of investigations related to the construction and the modification of supported ultrathin films and of non-woven fibre mats from blends containing cellulose derivatives. The field studied is of interdisciplinary interest and this work was also an effort to pave the way for future scientific collaboration.

7. REFERENCES

1. Feynman RP. **(1960)** There's plenty of room at the bottom. *Eng. Sci.* 23 (5): 22.

2. Taniguchi N. **(1974)** On the basic concept of 'nano-technology'. *Proceedings of the International Conference of Production Engineering, Tokyo, Japan*.

3. Whitesides GM. **(2005)** Nanoscience, Nanotechnology, and Chemistry. *Small* 1 (2): 172.

4. Dowling A, Clift R, Grobert N, Hutton D, Oliver R, O'Neill O, Pethica J, Pidgeon N, Porritt J, Ryan J, Seaton A, Tendler S, Welland M, Whatmore R. **(2004)** Nanoscience and nanotechnologies: opportunities and uncertainties. *A report by The Royal Society & The Royal Academy of Engineering*. Available from: http://www.nanotec.org.uk/finalReport.htm.

5. Binns C. Introduction to Nanoscience and Nanotechnology. Hoboken, NJ, USA: Wiley; 2010.

6. Vasile C,. Phase Behaviour. In: Kulshreshtha AK, Vasile C, editors. Handbook of polymer blends and composites, Vol 3 Shawbury, Shewsbury, Shropshire, UK: Rapra Technology; 2002. p. 65-101.

7. Ogawa H, Kanayac T, Nishida K, Matsuba G. **(2007)** Phase separation and dewetting in polymer blend thin films. *Eur. Phys. J., Special Topics* 141 (1): 189.

8. Klemm D, Philipp B, Heinze T, Heinze U, Wagenknecht W. Comprehensive Cellulose Chemistry. Volume 1, Fundamentals and Analytical Methods. Weinheim: VCH Verlag GmbH; 1998.

9. Klemm D, Kramer F, Moritz S, Lindström T, Ankerfors M, Gray D, Dorris A. **(2011)** Nanocelluloses: A New Family of Nature-Based Materials. *Angew. Chem., Int. Ed.* 50 (24): 5438.

10. Lehmann J. Carbohydrates: structure and biology. Stuttgart: Thieme; 1998.

11. Medronho B, Romano A, Miguel MG, Stigsson L, Lindman B. **(2012)** Rationalizing cellulose (in)solubility: reviewing basic physicochemical aspects and role of hydrophobic interactions. *Cellulose* 19 (3): 581.

12. Nehls I, Wagenknecht W, Philipp B, Stscherbina D. **(1994)** Characterization of cellulose and cellulose derivatives in solution by high resolution ^{13}C-NMR spectroscopy. *Prog. Polym. Sci.* 19 (1): 29.

13. Heux L, Dinand E, Vignon MR. **(1999)** Structural aspects in ultrathin cellulose microfibrils followed by 13C CP-MAS NMR. *Carbohydr. Polym.* 40 (2): 115.

14. Fleming K, Gray DG, Matthews S. **(2001)** Cellulose Crystallites. *Chem. Eur. J.* 7 (9): 1831.

15. Kontturi E, Tammelin T, Österberg M. **(2006)** Cellulose — model films and the fundamental approach. *Chem. Soc. Rev.* 35: 1287.

16. Postek MT, Vladár A, Dagata J, Farkas N, Ming B, Wagner R, Raman A, Moon RJ, Sabo R, Wegner TH, Beecher J. **(2011)** Development of the metrology and imaging of cellulose nanocrystals. *Meas. Sci. Technol.* 22 (2): 024005.

17. Heinze T, Liebert T. **(2001)** Unconventional methods in cellulose functionalization. *Prog. Polym. Sci.* 26 (9): 1689.

18. Klemm D, Einfeldt L. **(2001)** Structure design of polysaccharides: novel concepts, selective syntheses, high value applications. *Macromol. Symp.* 163 (1): 35.

19. Klemm D, Philipp B, Heinze T, Heinze U, Wagenknecht W. Systematics of Cellulose Derivatization. Comprehensive cellulose chemistry. Volume 2, Functionalization of Cellulose Weinheim: VCH; 1998. p. 1-314.

20. El Seoud OA, Heinze T. Organic esters of cellulose: new perspectives for old polymers. In: Heinze T, editor. Polysaccharides I: Structure, Characterization and Use Berlin: Springer; 2005. p. 103-149.

21. Fox SC, Li B, Xu D, Edgar KJ. **(2011)** Regioselective esterification and etherification of cellulose: a review. *Biomacromolecules* 12 (6): 1956.

22. Laine J, Lindström T, Nordmark GG, Risinger G. **(2000)** Studies on topochemical modification of cellulosic fibers. Part 1. Chemical conditions for the attachment of carboxymethyl cellulose onto fibers. *Nord. Pulp Pap. Res. J.* 15 (5): 520.

23. Filpponen I, Kontturi E, Nummelin S, Rosilo H, Kolehmainen E, Ikkala O, Laine J. **(2012)** Generic Method for Modular Surface Modification of Cellulosic Materials in Aqueous Medium by Sequential "Click"-Reaction and Adsorption. *Biomacromolecules* 13 (3): 736.

24. Park S, Venditti RA, Abrecht DG, Jameel H, Pawlak JJ, Lee JM. **(2007)** Surface and pore structure modification of cellulose fibers through cellulase treatment. *J. Appl. Polym. Sci.* 103 (6): 3833.

25. Saarinen T, Österberg M, Laine J. **(2008)** Adsorption of polyelectrolyte multilayers and complexes on silica and cellulose surfaces studied by QCM-D. *Colloids Surf., A* 330 (2-3): 134.

26. Schaub M, Wenz G, Wegner G, Stein A, Klemm D. **(1993)** Ultrathin films of cellulose on silicon wafers. *Adv. Mater.* 5 (12): 919.

27. Kontturi E, Thüne PC, Niemantsverdriet JW. **(2005)** Trimethylsilylcellulose/Polystyrene Blends as a Means To Construct Cellulose Domains on Cellulose. *Macromolecules* 38 (26): 10712.

28. Mormann W, Demeter J. **(1999)** Silylation of Cellulose with Hexamethyldisilazane in Liquid Ammonia First Examples of Completely Trimethylsilylated Cellulose. *Macromolecules* 32 (5): 1706.

29. Bontea D, Caruntu G, Aelenei N. **(2000)** The characterization of some silylcellulose derivatives by XRD measurements. *J. Macromol. Sci., Part A: Pure Appl. Chem.* 37 (4): 395.

30. Pawlowski WP, Gilbert RD, Fornes RE, Purrington ST. **(1988)** The liquid-crystalline properties of selected cellulose derivatives. *J. Polym. Sci., Part B: Polym. Phys.* 26 (5): 1101.

31. Cooper GK, Sandberg KR, Hinck JF. **(1981)** Trimethylsilyl cellulose as precursor to regenerated cellulose fiber. *J. Appl. Polym. Sci.* 26 (11): 3827.

32. Brydson J. Cellulose Plastics. Plastics Materials. 7th ed.: Elsevier; 1999. p. 613-634.

33. Liu H, Hsieh Y. **(2002)** Ultrafine fibrous cellulose membranes from electrospinning of cellulose acetate. *J. Polym. Sci., Part B: Polym. Phys.* 40 (18): 2119.

34. Buchanan CM, Gardner RM, Komarek RJ. **(1993)** Aerobic biodegradation of cellulose acetate. *J. Appl. Polym. Sci.* 47 (10): 1709.

35. Ishigaki T, Sugano W, Ike M, Taniguchi H, Goto T, Fujita M. **(2002)** Effect of UV irradiation on enzymatic degradation of cellulose acetate. *Polym. Degrad. Stab.* 78 (3): 505.

36. Walheim S, Schäffer E, Mlynek J, Steiner U. **(1999)** Nanophase-Separated Polymer Films as High-Performance Antireflection Coatings. *Science* 283 (5401): 520.

37. Nardes AM, Kemerink M, Janssen RAJ, Bastiaansen JAM, Kiggen NMM, Langeveld BMW, van Breemen, A. J. J. M., de Kok MM. **(2007)** Microscopic Understanding of the Anisotropic Conductivity of PEDOT:PSS Thin Films. *Adv. Mater.* 19 (9): 1196.

38. Decher G, Hong JD. **(1991)** Buildup of ultrathin multilayer films by a self-assembly process, 1 consecutive adsorption of anionic and cationic bipolar amphiphiles on charged surfaces. *Makromol. Chem., Macromol. Symp.* 46: 321.

39. Larson RG, Rehg TJ. Spin Coating. In: Kistler SF, Schweizer PM, editors. Liquid film coating : scientific principles and their technological implications London: Chapman & Hall; 1997. p. 709-739.

40. Choy K. **(2003)** Chemical vapour deposition of coatings. *Prog. Mater. Sci.* 48 (2): 57.

41. Peterson I. **(1990)** Langmuir-blodgett films. *J. Phys. D* 23 (4): 379.

42. Roman M. Model cellulosic surfaces: History and recent advances. In: Roman M, editor. Model cellulosic surfaces: ACS Publications; 2009. p. 3-53.

43. Norrman K, Ghanbari-Siahkali A, Larsen N. **(2005)** Studies of spin-coated polymer films. *Annu. Rep. Prog. Chem., Sect C* 101: 174.

44. Böltau M, Walheim S, Mlynek J, Krausch G, Steiner U. **(1998)** Surface-induced structure formation of polymer blends on patterned substrates. *Nature* 391 (6670): 877.

45. Emslie AG, Bonner FT, Peck LG. **(1958)** Flow of a viscous liquid on a rotating disk. *J. Appl. Phys.* 29 (5): 858.

46. Acrivos A, Shah M, Petersen E. **(1960)** On the Flow of a Non-Newtonian Liquid on a Rotating Disk. *J. Appl. Phys.* 31 (6): 963.

47. Meyerhofer D. **(1978)** Characteristics of resist films produced by spinning. *J. Appl. Phys.* 49 (7): 3993.

48. Bornside D, Macosko C, Scriven L. **(1987)** On the modeling of spin coating. *J. Imaging Technol.* 13 (4): 122.

49. Sczech R, Riegler H. **(2006)** Molecularly smooth cellulose surfaces for adhesion studies. *J. Colloid Interface Sci.* 301 (2): 376.

50. Kontturi E, Thüne PC, Niemantsverdriet JW. **(2003)** Cellulose model surfaces - simplified preparation by spin coating and characterization by X-ray photoelectron spectroscopy, infrared spectroscopy, and atomic force microscopy. *Langmuir* 19 (14): 5735.

51. Mi F, Shyu S, Wu Y, Lee S, Shyong J, Huang R. **(2001)** Fabrication and characterization of a sponge-like asymmetric chitosan membrane as a wound dressing. *Biomaterials* 22 (2): 165.

52. Berth G, Voigt A, Dautzenberg H, Donath E, Möhwald H. **(2002)** Polyelectrolyte complexes and layer-by-layer capsules from chitosan/chitosan sulfate. *Biomacromolecules* 3 (3): 579.

53. Lu C, Luo C, Cao W. **(2002)** Fabrication of ultrathin films based on chitosan and bovine serum albumin and their stability studied with the radio-labeled method. *Colloids Surf., B* 25 (1): 19.

54. Murray CA, Dutcher JR. **(2006)** Effect of changes in relative humidity and temperature on ultrathin chitosan films. *Biomacromolecules* 7 (12): 3460.

55. Fu J, Ji J, Yuan W, Shen J. **(2005)** Construction of anti-adhesive and antibacterial multilayer films via layer-by-layer assembly of heparin and chitosan. *Biomaterials* 26 (33): 6684.

56. Kreke MR, Badami AS, Brady JB, Michael Akers R, Goldstein AS. **(2005)** Modulation of protein adsorption and cell adhesion by poly(allylamine hydrochloride) heparin films. *Biomaterials* 26 (16): 2975.

57. Horlacher T, Seeberger PH. **(2008)** Carbohydrate arrays as tools for research and diagnostics. *Chem. Soc. Rev.* 37 (7): 1414.

58. Boddohi S, Kipper MJ. **(2010)** Engineering Nanoassemblies of Polysaccharides. *Adv. Mater.* 22 (28): 2998.

59. Wittenberg NJ, Im H, Johnson TW, Xu X, Warrington AE, Rodriguez M, Oh S. **(2011)** Facile Assembly of Micro- and Nanoarrays for Sensing with Natural Cell Membranes. *ACS Nano* 5 (9): 7555.

60. Thierry B, Kujawa P, Tkaczyk C, Winnik FM, Bilodeau L, Tabrizian M. **(2005)** Delivery Platform for Hydrophobic Drugs: Prodrug Approach Combined with Self-Assembled Multilayers. *J. Am. Chem. Soc.* 127 (6): 1626.

61. Schneider S, Feilen PJ, Slotty V, Kampfner D, Preuss S, Berger S, Beyer J, Pommersheim R. **(2001)** Multilayer capsules: a promising microencapsulation system for transplantation of pancreatic islets. *Biomaterials* 22 (14): 1961.

62. Ahola S, Salmi J, Johansson LS, Laine J, Österberg M. **(2008)** Model Films from Native Cellulose Nanofibrils. Preparation, Swelling, and Surface Interactions. *Biomacromolecules* 9 (4): 1273.

63. Edgar CD, Gray DG. **(2003)** Smooth model cellulose I surfaces from nanocrystal suspensions. *Cellulose* 10 (4): 299.

64. Eriksson M, Notley SM, Wågberg L. **(2005)** The influence on paper strength properties when building multilayers of weak polyelectrolytes onto wood fibers. *J. Colloid Interface Sci.* 292 (1): 38.

65. Fält S, Wågberg L, Vesterlind E, Larsson P. **(2004)** Model films of cellulose II – improved preparation method and characterization of the cellulose film. *Cellulose* 11 (2): 151.

66. McCormick CL, Callais PA, Hutchinson Jr BH. **(1985)** Solution studies of cellulose in lithium chloride and N, N-dimethylacetamide. *Macromolecules* 18 (12): 2394.

67. Rosenau T, Potthast A, Sixta H, Kosma P. **(2001)** The chemistry of side reactions and byproduct formation in the system NMMO/cellulose (Lyocell process). *Prog. Polym. Sci.* 26 (9): 1763.

68. Lua YY, Cao X, Rohrs BR, Aldrich DS. **(2007)** Surface characterizations of spin-coated films of ethylcellulose and hydroxypropyl methylcellulose blends. *Langmuir* 23 (8): 4286.

69. Abitbol T, Gray D. **(2007)** CdSe/ZnS QDs Embedded in Cellulose Triacetate Films with Hydrophilic Surfaces. *Chem. Mater.* 19 (17): 4270.

70. Kasai W, Kondo T. **(2004)** Fabrication of Honeycomb-Patterned Cellulose Films. *Macromol. Biosci.* 4 (1): 17.

71. Amim Jr J, Kosaka P, Petri D. **(2008)** Characteristics of thin cellulose ester films spin-coated from acetone and ethyl acetate solutions. *Cellulose* 15 (4): 527.

72. Palla-Papavlu A, Rusen L, Dinca V, Filipescu M, Lippert T, Dinescu M. **(2014)** Characterization of ethylcellulose and hydroxypropyl methylcellulose thin films deposited by matrix-assisted pulsed laser evaporation. *Appl. Surf. Sci.* 302: 87.

73. Buchholz V, Wegner G, Stemme S, Ödberg L. **(1996)** Regeneration, derivatization and utilization of cellulose in ultrathin films. *Adv. Mater.* 8 (5): 399.

74. Holmberg M, Berg J, Stemme S, Ödberg L, Rasmusson J, Claesson P. **(1997)** Surface force studies of Langmuir–Blodgett cellulose films. *J. Colloid Interface Sci.* 186 (2): 369.

75. Geffroy C, Labeau M, Wong K, Cabane B, Cohen Stuart M. **(2000)** Kinetics of adsorption of polyvinylamine onto cellulose. *Colloids Surf., A* 172 (1): 47.

76. Kontturi E, Thüne P, Niemantsverdriet J. **(2003)** Novel method for preparing cellulose model surfaces by spin coating. *Polymer* 44 (13): 3621.

77. Rossetti FF, Panagiotou P, Rehfeldt F, Schneck E, Dommach M, Funari SS, Timmann A, Müller-Buschbaum P, Tanaka M. **(2008)** Structures of regenerated cellulose films revealed by grazing incidence small-angle x-ray scattering. *Biointerphases* 3 (4): 117.

78. Mohan T, Kargl R, Doliška A, Vesel A, Köstler S, Ribitsch V, Stana-Kleinschek K. **(2011)** Wettability and surface composition of partly and fully regenerated cellulose thin films from trimethylsilyl cellulose. *J. Colloid Interface Sci.* 358 (2): 604.

79. Mohan T, Kargl R, Köstler S, Doliška A, Findenig G, Ribitsch V, Stana-Kleinschek K. **(2012)** Functional polysaccharide conjugates for the preparation of microarrays. *ACS Appl. Mater. Interfaces* 4 (5): 2743.

80. Kontturi E, Johansson L, Kontturi KS, Ahonen P, Thune PC, Laine J. **(2007)** Cellulose Nanocrystal Submonolayers by Spin Coating. *Langmuir* 23 (19): 9674.

81. Rehfeldt F, Tanaka M. **(2003)** Hydration Forces in Ultrathin Films of Cellulose. *Langmuir* 19 (5): 1467.

82. Niinivaara E, Kontturi E. **(2014)** 2D Dendritic Fractal Patterns from an Amphiphilic Polysaccharide. *Soft Matter* 10 (11): 1801.

83. Park MS, Kim JK. **(2004)** Breath figure patterns prepared by spin coating in a dry environment. *Langmuir* 20 (13): 5347.

84. Kargl R, Mohan T, Köstler S, Spirk S, Doliška A, Stana-Kleinschek K, Ribitsch V. **(2013)** Functional patterning of biopolymer thin films using enzymes and lithographic methods. *Adv. Funct. Mater.* 23 (3): 308.

85. Utracki LA. Polymer blends handbook. Dordrecht: Kluwer Academic; 2002.

86. Budkowski A. **(1999)** Interfacial Phenomena in Thin Polymer Films: Phase Coexistence and Segregation. *Adv. Polym. Sci.* 148: 1.

87. Hu W. Polymer Phase Separation. Polymer Physics. Springer Verlag; 2013. p. 167-186.

88. Higgins JS, Lipson JE, White RP. **(2010)** A simple approach to polymer mixture miscibility. *Phil. Trans. R. Soc. A* 368 (1914): 1009.

89. Bates F, Wignall G, Koehler W. **(1985)** Critical behavior of binary liquid mixtures of deuterated and protonated polymers. *Phys. Rev. Lett.* 55 (22): 2425.

90. Ebbens S, Hodgkinson R, Parnell AJ, Dunbar A, Martin SJ, Topham PD, Clarke N, Howse JR. **(2011)** In situ imaging and height reconstruction of phase separation processes in polymer blends during spin coating. *ACS Nano* 5 (6): 5124.

91. Walheim S, Böltau M, Mlynek J, Krausch G, Steiner U. **(1997)** Structure Formation via Polymer Demixing in Spin-Cast Films. *Macromolecules* 30 (17): 4995.

92. Binder K. **(1999)** Phase Transitions of Polymer Blends and Block Copolymer Melts in Thin Films. *Adv. Polym. Sci.* 138: 1.

93. Sprenger M, Walheim S, Budkowski A, Steiner U. **(2003)** Hierarchic structure formation in binary and ternary polymer blends. *Interface Sci.* 11 (2): 225.

94. Bucknall DG. **(2004)** Influence of interfaces on thin polymer film behaviour. *Prog. Mater. Sci.* 49: 713.

95. Young T. **(1805)** An Essay on the Cohesion of Fluids. *Philos. Trans. R. Soc. London* 95: 65.

96. Seemann R, Herminghaus S, Neto C, Schlagowski S, Podzimek D, Konrad R, Mantz H, Jacobs K. **(2005)** Dynamics and structure formation in thin polymer melt films. *J. Phys.: Concens. Matter* 17 (9): S267.

97. Krausch G. **(1997)** Dewetting at the interface between two immiscible polymers. *J. Phys.: Concens. Matter* 9 (37): 7741.

98. Reiter G. **(1993)** Unstable thin polymer films: Rupture and dewetting processes. *Langmuir* 9 (5): 1344.

99. Stange T, Evans D, Hendrickson W. **(1997)** Nucleation and growth of defects leading to dewetting of thin polymer films. *Langmuir* 13 (16): 4459.

100. Sharma A, Reiter G. **(1996)** Instability of thin polymer films on coated substrates: rupture, dewetting, and drop formation. *J. Colloid Interface Sci.* 178 (2): 383.

101. Higgins A, Jones R. **(2000)** Anisotropic spinodal dewetting as a route to self-assembly of patterned surfaces. *Nature* 404 (6777): 476.

102. Jacobs K, Herminghaus S, Mecke KR. **(1998)** Thin liquid polymer films rupture via defects. *Langmuir* 14 (4): 965.

103. Thiele U, Mertig M, Pompe W. **(1998)** Dewetting of an evaporating thin liquid film: Heterogeneous nucleation and surface instability. *Phys. Rev. Lett.* 80 (13): 2869.

104. Jones RAL. **(1999)** The dynamics of thin polymer films. *Curr. Opin. Colloid Interface Sci.* 4: 153.

105. Heriot SY, Jones RAL. **(2005)** An interfacial instability in a transient wetting layer leads to lateral phase separation in thin spin-cast polymer-blend films. *Nat. Mater.* 4: 782.

106. Tanaka K, Takahara A, Kajiyama T. **(1996)** Film thickness dependence of the surface structure of immiscible polystyrene/poly (methyl methacrylate) blends. *Macromolecules* 29 (9): 3232.

107. Ton-That C, Shard A, Teare D, Bradley R. **(2001)** XPS and AFM surface studies of solvent-cast PS/PMMA blends. *Polymer* 42 (3): 1121.

108. Jukes PC, Heriot SY, Sharp JS, Jones RA. **(2005)** Time-resolved light scattering studies of phase separation in thin film semiconducting polymer blends during spin-coating. *Macromolecules* 38 (6): 2030.

109. Affrossman S, Stamm M. **(2000)** The effect of molecular weight on the topography of thin films of blends of poly (4-bromostyrene) and polystyrene. *Colloid Polym. Sci.* 278 (9): 888.

110. Affrossman S, O'Neill SA, Stamm M. **(1998)** Topography and surface composition of thin films of blends of polystyrene with brominated polystyrenes: effects of varying the degree of bromination and annealing. *Macromolecules* 31 (18): 6280.

111. Dunbar A, Mokarian-Tabari P, Parnell AJ, Martin SJ, Skoda M, Jones R. **(2010)** A solution concentration dependent transition from self-stratification to lateral phase separation in spin-cast PS: d-PMMA thin films. *Eur. Phys. J. E* 31 (4): 369.

112. Malkan SR. Overview of Nonwovens. In: Turbak AF, editor. Nonwovens : theory, process, performance, and testing Atlanta, GA, USA: TAPPI; 1993. p. 1-10.

113. Fahrbach E, Schaut G, Wegmann A. Nonwoven Fabrics. In: Bohnet M, editor. Ullmann's Encyclopedia of Industrial Chemistry. 7th ed.: Wiley; 2008. p. 585-608.

114. Ramakrishna S, Fujihara K, Teo W, Yong T, Ma Z, Ramaseshan R. **(2006)** Electrospun nanofibers: solving global issues. *Mater. Today* 9 (3): 40.

115. Hagewood J, Wilkie A. **(2003)** Advances in sub-micron fiber production. *Nonwovens world* 12 (2): 69.

116. Malkan SR, Wadsworth LC. Melt-blowing process. In: Turbak AF, editor. Nonwovens : theory, process, performance, and testing Atlanta, GA, USA: TAPPI; 1993. p. 181-185.

117. Greiner A, Wendorff JH. **(2007)** Electrospinning: A Fascinating Method for the Preparation of Ultrathin Fibers. *Angew. Chem., Int. Ed.* 46 (30): 5670.

118. Formhals A, Schreiber-Gastell R, inventors. Process and apparatus for preparing artificial threads. U.S. Pat 1 975 504. 1934 2 October.

119. Doshi J, Reneker DH. **(1995)** Electrospinning process and applications of electrospun fibers. *J. Electrostatics* 35 (2-3): 151.

120. Ramakrishna S, Jose R, Archana PS, Nair AS, Balamurugan R, Venugopal J, Teo WE. **(2010)** Science and engineering of electrospun nanofibers for advances in clean energy, water filtration, and regenerative medicine. *J. Mater. Sci.* 45 (23): 6283.

121. Reneker DH, Chun I. **(1996)** Nanometre diameter fibres of polymer, produced by electrospinning. *Nanotechnology* 7 (3): 216.

122. Luo CJ, Stoyanov SD, Stride E, Pelan E, Edirisinghe M. **(2012)** Electrospinning versus fibre production methods: from specifics to technological convergence. *Chem. Soc. Rev.* 41 (13): 4708.

123. W E Teo and SR. **(2006)** A review on electrospinning design and nanofibre assemblies. *Nanotechnology* 17 (14): R89.

124. Li D, Xia Y. **(2004)** Electrospinning of Nanofibers: Reinventing the Wheel? *Adv. Mater.* 16 (14): 1151.

125. Schiffman JD, Schauer CL. **(2008)** A Review: Electrospinning of Biopolymer Nanofibers and their Applications. *Polym. Rev.* 48 (2): 317.

126. Taylor G. **(1964)** Disintegration of water drops in an electric field. *Proc. R. Soc. Lond. A* 280 (1382): 383.

127. Reneker DH, Yarin AL, Fong H, Koombhongse S. **(2000)** Bending instability of electrically charged liquid jets of polymer solutions in electrospinning. *J. Appl. Phys.* 87: 4531.

128. Doshi J. **(2001)** Nanofiber-Based Nonwoven Composites: Properties and Applications. *Nonwovens world* 10 (4): 64.

129. Rodríguez K, Sundberg J, Gatenholm P, Renneckar S. **(2012)** Electrospun nanofibrous cellulose scaffolds with controlled microarchitecture. *Carbohydr. Polym.* 100: 143.

130. Kulpinski P. **(2005)** Cellulose nanofibers prepared by the N-methylmorpholine-N-oxide method. *J. Appl. Polym. Sci.* 98 (4): 1855.

131. Kim C, Frey MW, Marquez M, Joo YL. **(2005)** Preparation of submicron-scale, electrospun cellulose fibers via direct dissolution. *J. Polym. Sci., Part B: Polym. Phys.* 43 (13): 1673.

132. Quan S, Kang S, Chin I. **(2010)** Characterization of cellulose fibers electrospun using ionic liquid. *Cellulose* 17 (2): 223.

133. Jaeger R, Bergshoef MM, Batlle CMI, Schönherr H, Julius Vancso G. **(1998)** Electrospinning of ultra-thin polymer fibers. *Macromol. Symp.* 127 (1): 141.

134. Frey MW. **(2008)** Electrospinning Cellulose and Cellulose Derivatives. *Polym. Rev.* 48: 378.

135. Frenot A, Henriksson MW, Walkenström P. **(2007)** Electrospinning of cellulose-based nanofibers. *J. Appl. Polym. Sci.* 103 (3): 1473.

136. Wu X, Wang L, Yu H, Huang Y. **(2005)** Effect of solvent on morphology of electrospinning ethyl cellulose fibers. *J. Appl. Polym. Sci.* 97 (3): 1292.

137. Ding B, Kimura E, Sato T, Fujita S, Shiratori S. **(2004)** Fabrication of blend biodegradable nanofibrous nonwoven mats via multi-jet electrospinning. *Polymer* 45 (6): 1895.

138. Kontturi E, Suchy M, Penttila P, Jean B, Pirkkalainen K, Torkkeli M, Serimaa R. **(2011)** Amorphous Characteristics of an Ultrathin Cellulose Film. *Biomacromolecules* 12 (3): 770.

139. Greber G, Paschinger O. **(1981)** Silylderivate der cellulose. *Papier* 35 (12): 547.

140. Binnig G, Rohrer H, Gerber C, Weibel E. **(1982)** Surface studies by scanning tunneling microscopy. *Phys. Rev. Lett.* 49 (1): 57.

141. Binnig G, Quate CF, Gerber C. **(1986)** Atomic force microscope. *Phys. Rev. Lett.* 56 (9): 930.

142. Gross L, Mohn F, Moll N, Liljeroth P, Meyer G. **(2009)** The chemical structure of a molecule resolved by atomic force microscopy. *Science* 325 (5944): 1110.

143. Hunger K, Mischke P, Rieper W. Surface and Thin-Film Analysis, 5. Scanning Probe Microscopy. In: Bohnet M, editor. Ullmann's Encyclopedia of Industrial Chemistry. 7th ed.: Wiley; 2008. p. 419-430.

144. Yuan Y, Lee TR. Contact Angle and Wetting Properties. In: Bracco G, Holst B, editors. Surface Science Techniques Berlin: Springer Berlin Heidelberg; 2013. p. 3-34.

145. Snoeijer JH, Andreotti B. **(2008)** A microscopic view on contact angle selection. *Phys. Fluids* 20 (5): 057101-1.

146. Wenzel RN. **(1936)** Resistance of solid surfaces to wetting by water. *Ind. Eng. Chem.* 28 (8): 988.

147. Cassie AB, Baxter S. **(1944)** Wettability of porous surfaces. *Trans. Faraday Soc.* 40: 546.

148. Brandon S, Haimovich N, Yeger E, Marmur A. **(2003)** Partial wetting of chemically patterned surfaces: The effect of drop size. *J. Colloid Interface Sci.* 263 (1): 237.

149. Marmur A. **(2003)** Wetting on Hydrophobic Rough Surfaces: To Be Heterogeneous or Not To Be? *Langmuir* 19 (20): 8343.

150. Quéré D, Lafuma A, Bico J. **(2003)** Slippy and sticky microtextured solids. *Nanotechnology* 14 (10): 1109.

151. McHale G, Shirtcliffe NJ, Newton MI. **(2004)** Contact-Angle Hysteresis on Super-Hydrophobic Surfaces. *Langmuir* 20 (23): 10146.

152. Wang S, Jiang L. **(2007)** Definition of Superhydrophobic States. *Adv. Mater.* 19 (21): 3423.

153. Gao L, McCarthy TJ. **(2006)** Contact Angle Hysteresis Explained. *Langmuir* 22 (14): 6234.

154. Gao L, McCarthy TJ. **(2007)** How Wenzel and Cassie Were Wrong. *Langmuir* 23 (7): 3762.

155. Gao L, McCarthy TJ. **(2009)** An Attempt to Correct the Faulty Intuition Perpetuated by the Wenzel and Cassie Laws. *Langmuir* 25 (13): 7249.

156. de Gennes PG. **(1985)** Wetting: statics and dynamics. *Rev. Mod. Phys.* 57 (3): 827.

157. Dorris GM, Gray DG. **(1978)** The surface analysis of paper and wood fibers by Esca-electron spectroscopy for chemical analysis - I. Applications to cellulose and lignin. *Cellul. Chem. Technol.* 12: 9.

158. Beamson G, Briggs D. High Resolution XPS of Organic Polymers. Chichester: John Wiley & Sons; 1992.

159. Niemantsverdriet JW. Spectroscopy in catalysis: an introduction. 3rd rev. ed. Weinheim: Wiley-VCH; 2007.

160. Rodahl M, Höök F, Krozer A, Brzezinski P, Kasemo B. **(1995)** Quartz crystal microbalance setup for frequency and Q-factor measurements in gaseous and liquid environments. *Rev. Sci. Instrum.* 66 (7): 3924.

161. Sauerbrey GZ. **(1959)** Use of quartz vibration for weighing thin films on a microbalance. *Phys. C: Part. Fields* 2 (155): 206.

162. Höök F, Rodahl M, Brzezinski P, Kasemo B. **(1998)** Energy Dissipation Kinetics for Protein and Antibody-Antigen Adsorption under Shear Oscillation on a Quartz Crystal Microbalance. *Langmuir* 14 (4): 729.

163. Johannsmann D, Mathauer K, Wegner G, Knoll W. **(1992)** Viscoelastic properties of thin films probed with a quartz-crystal resonator. *Phys. Rev. B* 46 (12): 7808.

164. Voinova MV, Rodahl M, Jonson M, Kasemo B. **(1999)** Viscoelastic Acoustic Response of Layered Polymer Films at Fluid-Solid Interfaces: Continuum Mechanics Approach. *Phys. Scripta* 59 (5): 391.

165. Orelma H, Filpponen I, Johansson L, Laine J, Rojas OJ. **(2011)** Modification of Cellulose Films by Adsorption of CMC and Chitosan for Controlled Attachment of Biomolecules. *Biomacromolecules* 12 (12): 4311.

166. Wang P, Koberstein JT. **(2004)** Morphology of Immiscible Polymer Blend Thin Films Prepared by Spin-Coating. *Macromolecules* 37 (15): 5671.

167. Müller-Buschbaum P, Gutmann JS, Stamm M. **(2000)** Influence of Blend Composition on Phase Separation and Dewetting of Thin Polymer Blend Films. *Macromolecules* 33 (13): 4886.

168. Iyer KS, Luzinov I. **(2003)** Surface Morphology of Mechanically Heterogeneous Ultrathin Polymer Films. *Langmuir* 19 (1): 118.

169. Gu X, Gunkel I, Russell TP. **(2013)** Pattern transfer using block copolymers. *Philos. Trans. A. Math. Phys. Eng. Sci.* 371 (2000): 20120306.

170. Panchagnula MV, Vedantam S. **(2007)** Comment on How Wenzel and Cassie Were Wrong by Gao and McCarthy. *Langmuir* 23 (26): 13242.

171. Tammelin T, Saarinen T, Österberg M, Laine J. **(2006)** Preparation of Langmuir/Blodgett-cellulose surfaces by using horizontal dipping procedure. Application for polyelectrolyte adsorption studies performed with QCM-D. *Cellulose* 13 (5): 519.

172. Aulin C, Ahola S, Josefsson P, Nishino T, Hirose Y, Österberg M, Wågberg L. **(2009)** Nanoscale Cellulose Films with Different Crystallinities and Mesostructures-Their Surface Properties and Interaction with Water. *Langmuir* 25 (13): 7675.

173. Mazeau K, Rivet A. **(2008)** Wetting the (110) and (100) surfaces of Iβ cellulose studied by molecular dynamics. *Biomacromolecules* 9 (4): 1352.

174. Yamane C, Aoyagi T, Ago M, Sato K, Okajima K, Takahashi T. **(2006)** Two different surface properties of regenerated cellulose due to structural anisotropy. *Polym. J.* 38 (8): 819.

175. Mohan T, Ristić T, Kargl R, Doliska A, Köstler S, Ribitsch V, Marn J, Spirk S, Stana-Kleinschek K. **(2013)** Cationically rendered biopolymer surfaces for high protein affinity support matrices. *Chem. Commun.* 49 (98): 11530.

176. Burchard W. **(2003)** Solubility and Solution Structure of Cellulose Derivatives. *Cellulose* 10 (3): 213.

177. Mistark PA, Park S, Yalcin SE, Lee DH, Yavuzcetin O, Tuominen MT, Russell TP, Achermann M. **(2009)** Block-copolymer-based plasmonic nanostructures. *ACS Nano* 3 (12): 3987.

178. Blunt MO, Suvakov M, Pulizzi F, Martin CP, Pauliac-Vaujour E, Stannard A, Rushforth AW, Tadic B, Moriarty P. **(2007)** Charge Transport in Cellular Nanoparticle Networks: Meandering through Nanoscale Mazes. *Nano Lett.* 7 (4): 855.

179. Cao G. Nanostructures and Nanomaterials - Synthesis, Properties and Applications. London, UK: Imperial College Press; 2004.

180. Tanaka M, Wong AP, Rehfeldt F, Tutus M, Kaufmann S. **(2004)** Selective Deposition of Native Cell Membranes on Biocompatible Micropatterns. *J. Am. Chem. Soc.* 126 (10): 3257.

181. Lavenson D, Tozzi E, McCarthy M, Powell R. **(2012)** Effective diffusivities of BSA in cellulosic fiber beds measured with magnetic resonance imaging. *Cellulose* 19(4): 1085.

182. Jaczewska J, Budkowski A, Bernasik A, Raptis I, Raczkowska J, Goustouridis D, Rysz J, Sanopoulou M. **(2007)** Humidity and solvent effects in spin coated polythiophene–polystyrene blends. *J. Appl. Polym. Sci.* 105 (1): 67.

183. Bunz UHF. **(2006)** Breath Figures as a Dynamic Templating Method for Polymers and Nanomaterials. *Adv. Mater.* 18 (8): 973.

184. Hecht U, Schilz C, Stratmann M. **(1998)** Influence of relative humidity during film formation processes on the structure of ultrathin polymeric films. *Langmuir* 14 (23): 6743.

185. Madej W, Budkowski A, Raczkowska J, Rysz J. **(2008)** Breath figures in polymer and polymer blend films spin-coated in dry and humid ambience. *Langmuir* 24 (7): 3517.

186. Park MS, Joo W, Kim JK. **(2006)** Porous structures of polymer films prepared by spin coating with mixed solvents under humid condition. *Langmuir* 22 (10): 4594.

187. Lee S, Kang H, Kim YS, Char K. **(2003)** Hierarchical surface topography in block copolymer thin films induced by residual solvent. *Macromolecules* 36 (13): 4907.

188. Thickett SC, Harris A, Neto C. **(2010)** Interplay between Dewetting and Layer Inversion in Poly (4-vinylpyridine)/Polystyrene Bilayers. *Langmuir* 26 (20): 15989.

189. Yoon BK, Huh J, Kim H, Hong J, Park C. **(2006)** Ordered patterns of microimprinted bilayer polymer films with controlled dewetting and layer inversion. *Macromolecules* 39 (3): 901.

190. Steiner U, Klein J, Fetters L. **(1994)** Surface phase inversion in finite-sized binary mixtures. *Phys. Rev. Lett.* 72 (10): 1498.

191. Back EL, Salmén NL. **(1982)** Glass transitions of wood components hold implications for molding and pulping processes. *Tappi* 65 (7): 107.

192. Keddie J, Jones R, Cory R. **(1994)** Size-dependent depression of the glass transition temperature in polymer films. *Europhys. Lett.* 27 (1): 59.

193. Bernasik A, Haberko J, Włodarczyk-Miśkiewicz J, Raczkowska J, Łużny W, Budkowski A, Kowalski K, Rysz J. **(2005)** Influence of humid atmosphere on phase separation in polyaniline–polystyrene thin films. *Synth. Met.* 155 (3): 516.

194. Megelski S, Stephens JS, Chase DB, Rabolt JF. **(2002)** Micro- and Nanostructured Surface Morphology on Electrospun Polymer Fibers. *Macromolecules* 35 (22): 8456.

195. Bognitzki M, Czado W, Frese T, Schaper A, Hellwig M, Steinhart M, Greiner A, Wendorff JH. **(2001)** Nanostructured Fibers via Electrospinning. *Adv. Mater.* 13 (1): 70.

196. McCann JT, Marquez M, Xia Y. **(2006)** Highly Porous Fibers by Electrospinning into a Cryogenic Liquid. *J. Am. Chem. Soc.* 128 (5): 1436.

197. Li D, Xia Y. **(2004)** Direct Fabrication of Composite and Ceramic Hollow Nanofibers by Electrospinning. *Nano Lett.* 4 (5): 933.

198. Bognitzki M, Frese T, Steinhart M, Greiner A, Wendorff JH, Schaper A, Hellwig M. **(2001)** Preparation of fibers with nanoscaled morphologies: Electrospinning of polymer blends. *Polym. Eng. Sci.* 41 (6): 982.

199. Hohman MM, Shin M, Rutledge G, Brenner MP. **(2001)** Electrospinning and electrically forced jets. I. Stability theory. *Phys. Fluids* 13 (8): 2201.

200. Feng L, Zhang Y, Xi J, Zhu Y, Wang N, Xia F, Jiang L. **(2008)** Petal Effect: A Superhydrophobic State with High Adhesive Force. *Langmuir* 24 (8): 4114.

201. Balu B, Breedveld V, Hess DW. **(2008)** Fabrication of "Roll-of" and "Sticky" Superhydrophobic Cellulose Surfaces via Plasma Processing. *Langmuir* 24 (9): 4785.

202. Pisuchpen T, Chaim-ngoen N, Intasanta N, Supaphol P, Hoven VP. **(2011)** Tuning Hydrophobicity and Water Adhesion by Electrospinning and Silanization. *Langmuir* 27 (7): 3654.

203. Uchida K, Nishikawa N, Izumi N, Yamazoe S, Mayama H, Kojima Y, Yokojima S, Nakamura S, Tsujii K, Irie M. **(2010)** Phototunable Diarylethene Microcrystalline Surfaces: Lotus and Petal Effects upon Wetting. *Angew. Chem., Int. Ed.* 49 (34): 5942.

204. Onda T, Shibuichi S, Satoh N, Tsujii K. **(1996)** Super-Water-Repellent Fractal Surfaces. *Langmuir* 12 (9): 2125.

205. Roach P, Shirtcliffe NJ, Newton MI. **(2008)** Progess in superhydrophobic surface development. *Soft Matter* 4 (2): 224.

206. Harton SE, Lüning J, Betz H, Ade H. **(2006)** Polystyrene/poly (methyl methacrylate) blends in the presence of cyclohexane: Selective solvent washing or equilibrium adsorption?. *Macromolecules* 39 (22): 7729.

Aalto-DD 87/2014

ISBN 978-952-60-5730-9
ISBN 978-952-60-5731-6 (pdf)
ISSN-L 1799-4934
ISSN 1799-4934
ISSN 1799-4942 (pdf)

Aalto University
School of Chemical Technology
Department of Forest Products Technology
www.aalto.fi

BUSINESS +
ECONOMY

ART +
DESIGN +
ARCHITECTURE

SCIENCE +
TECHNOLOGY

CROSSOVER

DOCTORAL
DISSERTATIONS